Catarina Filipa Braz Rijo

Licenciada em Ciências de Micro e Nanotecnologias

A paper-based low-cost label-free biosensing silver core-gold shell nanostructure for SERS to be applied to breast cancer diagnostics

Dissertação para obtenção do Grau de Mestre em

Engenharia de Micro e Nanotecnologias

Orientador: Elvira Maria Correia Fortunato, Professora catedrática, FCT-UNL

Co-orientador: Bruno Costa-Silva, Investigador, Fundação Champalimaud

Júri:

Presidente:

Arguente(s):

Vogal(ais):

FACULDADE DE CIÊNCIAS E TECNOLOGIA
UNIVERSIDADE NOVA DE LISBOA

Março 2018

A paper-based low-cost label-free biosensing silver core-gold shell nanostructure for SERS to be applied to breast cancer diagnostics

"One of the greatest discoveries a man makes, one of his great surprises, is to find he can do what he was afraid he couldn't do."

— Henry Ford

Acknowledgement

Antes de mais gostaria de agradecer à Faculdade de Ciências e Tecnologias da Universidade Nova de Lisboa que foi a minha casa em todos estes anos necessários para a conclusão do curso. Um agradecimento especial também ao Departamento de Ciências dos Materiais e a todos os excelentes professores que nestes anos me ensinaram, não só coisas técnicas, mas também várias vezes no aconselharam para sermos pessoas melhores na nossa vida.

Um especial obrigado ao professor Rodrigo Martins que tornou possível a minha formação neste curso, assim como o melhoramento do mesmo. Também à professora Elvira Fortunato por toda a sua disponibilidade para ajudar e orientação durante o período de realização da tese e ao longo de todo o curso. Também queria agradecer ao Dr. Bruno Costa-Silva pela oportunidade de trabalhar juntamente com a sua equipa na Fundação Champalimaud e ao Cristian Bodo pela sua paciência e disponibilidade no esclarecimento de dúvidas e vontade de ajudar.

Ao CENIMAT e toda a sua equipa, desde a professores a funcionários da secretaria. À Sónia Pereira e à Alexandra Gonçalves por ajudarem sempre que precisava de reagentes e caixas de Petri, pelas conversas de ocasião e por todas a chamadas de atenção que me fizeram que só contribuíram para me tornar uma pessoa melhor e mais atenta. À Carolina Marques que também esteve sempre disponível para ajudar e orientar nas tarefas e solucionadora de todos os problemas que tinha no Raman… À Professora Joana Pinho pelos resultados de DRX que não marquei mas a professora fez na mesma (ahah) Ao Jonas Deuermier por ser uma pessoa sempre disponível para ajudar e mais importante que tudo, sempre preocupado que a sua explicação em qualquer assunto fosse bem entendida! Também quero agradecer à Daniela Gomes, por muitas vezes, às 8h da manhã, estar a tentar tirar imagens de fibras de papel com nanopartículas com o SEM semi-estragado e as fibras desintegrarem (literalmente). Também à Raquel Água que foi muito importante no início do meu trabalho transmitindo-me conhecimentos essenciais tanto individualmente, como em reuniões, que me ajudaram a organizar as minhas tarefas. A todos os meus colegas que partilharam o laboratório comigo e sobreviveram às obras, obrigado!! Especialmente agradeço à minha querida amiga Catarina Costa que desde o dia 1 desta jornada se manteve como uma fiel amiga e companheira e que sempre esteve lá para mim.

A todos os amigos (que se tornaram família) que tive o prazer de conhecer. Ao meu grande amigo Marco Rodrigues, que mesmo desaparecido na maior parte do tempo, cada conversa com ele parecia que era como se tivéssemos sempre juntos. Ao Xavi, ao Centeno, ao Nano, ao Casa Branca e ao Narciso por fazerem parte de um grupo de amigos de Faculdade sempre prontos para beber aquela jola às cinco da tarde, por serem todos diferentes à sua maneira e por serem verdadeiros amigos!! À minha querida amiga Lauríssima, a amiga que demorei a conhecer mas desde que conheci nunca mais larguei, que se tornou a minha companheira de todas as horas e tenho a certeza que será uma amizade que levarei para a vida toda até termos filhos e os nossos filhos terem filhos. Orgulho-me em dizer que principalmente levo bons amigos de toda esta experiência, mas também gostava de salientar todas as pessoas que de alguma forma contribuíram para o meu trajeto, mesmo que já não nos falemos, porque sem eles não seria a pessoa que sou agora e acreditem que só guardo memórias boas!!

Aos meus amigos do Algarve que sempre me incentivaram a seguir os meus sonhos e que estão sempre lá para mim, mesmo havendo uma distância de 300 km a separar-nos… À minha grande, grande amiga Ana Beatriz Lopes, que me acompanha desde a primária (como é que é possível?) e que faz parte de quase todas as minhas memórias importantes, tanto boas, como más, é a minha metade! Ás minhas amigas Gabby Ferreira, Rita Martins pela amizade e boleias até ao Algarve e Ana Rita Cardoso. À Ana Rita era impossível escrever por palavras o quanto estou

grata por tudo o que ela fez por mim, às vezes até sem se aperceber. Ao Pedro Monteiro e todas as meninas que fizeram parte do grupo de teatro TV (Teatro Vilão), foram sem dúvida os melhores 4 anos da minha vida. A toda a gente que recentemente conheci e me ajudaram a ultrapassar certos momentos mais tristes e que estiveram comigo em outros de felicidade extrema.

Agora ao mais importante, à minha família, que ficou mais pequenina este ano, mas sem dúvida mais unida. À minha Tia Maria Pereira, mais conhecida por Joaquina, que já não está entre nós, mas que foi tão importante no meu crescimento pessoal enquanto ser humano, ensinou-me, com a doçura e jeito especial dela, a escutar os mais velhos e receber o amor e sabedoria dos mesmos. Tenho saudades dela! À minha mãe não tenho palavras para agradecer, todo o amor e carinho que me deu. É incalculável, todo o esforço que a vi fazer por mim, nunca conseguirei agradecer. Todos os taparweres de comida que ela me fez, todos os sacrifícios daqueles tempos difíceis que parecia que não íamos conseguir, mas conseguimos, obrigado, és a minha melhor amiga. Ao meu pai que acreditou em mim, que foi e é o pilar da nossa família, por sempre ter as palavras que mais me acalmavam quando achava que não ia conseguir, e por ser aquele que eu mais quero que tenha orgulho em mim! Amo-vos muito!! Não posso deixar de agradecer à minha pessoa favorita: o meu irmão Diogo. Aquele que foi o descuido que fez mais sentido na nossa família, não sei como consigo, mas o meu amor por ele é maior do que o meu próprio ser. É a pessoa que me completa e às vezes sem falar me ajuda mais do que qualquer pessoa, pelo seu olhar doce e enorme preocupação para comigo. Também um agradecimento especial ao resto da minha família que querem sempre o melhor para mim, sem vocês também não seria possível.

A todas as pessoas que aqui referi, e a outras tantas que não referi, espero que me continuem a acompanhar ao longo da minha vida que acaba de começar.

Abstract

Breast cancer (BCa) is one of the most common and deadly diseases in women worldwide. In 2018, 2.1 million cases were diagnosed with BCa from which 626,679 women died. Therefore, an early diagnosis is imperative for treatment and a cure success rate. Recent studies have concluded that exosomes can be used as biomarkers, since they participate in the communication between cells, carrying genetic information from the mother cells.

Common methods of detection of exosomes as Enzyme-Linked Immunosorbent Assays (ELISA) are used, however, large amounts of highly concentrated sample, special preparation and labelling processes are required. As an alternative, Raman Spectroscopy stands out as a low-cost, simple and fast detection method that leads to a less invasive real sample collection and sample preparation. Low sample volumes are needed due to surface enhancement signal (SERS). However commercial SERS substrate for these measures present high cost and low shelf-life.

In this work, Ag-core-Au-shell bimetallic nanoparticles were directly synthesized on paper substrates (Whatman and Office paper) through two-stage successive ionic layer absorption and reaction (SILAR) techniques and tested as SERS substrates. Enhancement factors (EF) from 10^4 to 10^5 were reached and, for both substrates the Limit of Detection (LOD) was calculated as 10^{-11} M R6G.

Non-tumoral (MCF-10A) and tumoral (MDA-MB-231) exosomes from breast cells were tested on the optimized substrates and Raman spectra were analysed by a statistical method called PCA (Principal Component Analysis). The data was successfully grouped with 95% confidence confirming its potential as a low-cost, label-free point-of-care test chip for the early diagnosis of breast cancer diseases.

Keywords: SILAR fabrication, bimetallic Ag@AuNPs, SERS, cellulose fibbers, PCA, exosomes

Resumo

O cancro da mama é a doença mais comum e mortal nas em todo o mundo, em 2018, 2.1 milhões de casos foram diagnosticados aos quais 626,679 mulheres acabaram por morrer. Consequentemente, é necessário que haja um diagnóstico precoce para o tratamento e sucesso na cura. Estudos recentes concluíram que exossomas podem ser usados como biomarcadores, uma vez que participam na comunicação entre células, deixando informação genética proveniente da célula mãe.

Métodos como Ensaios de Imunoadsorção Enzimática (ELISA) são normalmente usados, no entanto são necessárias grandes quantidades de amostra altamente concentrada, preparações especiais da amostra e processos de rotulagem.

Como alternativa, a Espectroscopia de Raman destaca-se como método mais barato, simples e de deteção rápida que implica uma coleta de amostra menos invasiva e preparação da amostra menos exigente, também um menor volume de amostra é necessário devido ao melhoramento de sinal à superfície (SERS). No entanto, substratos SERS comerciais apresentam elevado custo.

Neste trabalho, foram sintetizada nanopartículas bimetálicas Ag-núcleo-Au-concha diretamente nas fibras do papel (papel Whatman e de escritório) através da técnica de absorção e reação sucessiva de camada iónica (SILAR) e testado como substratos SERS. *Enhencement Factors* (EF) obtidos foram de 10^4 e 10^5 e para ambos os substratos, o limite de deteção (LOD) foi de 10^{-11} M R6G.

Exossomas saudávies (MCF-10A) e tumorais (MDA-MB-231) provenientes de células tumorais foram testados nos substratos otimizados e os espectros Raman foram analisados através de um método estatístico chamado de PCA (Principal Component Analysis). Onde os dados foram agrupados com 95% de confiança, confirmando o seu potencial como técnica de diagnóstico do cancro da mana no local, com baixo custo e *label free*.

Palavras-chave: fabricação SILAR, nanopartículas bimetálicas, Ag@AuNPs, fibras de celulose, PCA, exossomas

Abbreviations

CENIMAT	Centro de Investigação de Materiais
BCa	Breast Cancer
MVBs	Multivesicular Bodeis
$AgNO_3$	Silver Nitrate
AgNPs	Silver nanoparticles
$HAuCl_4$	Gold (III) chloride hydrate
AuNPs	Gold nanoparticles
$NaBH_4$	Sodium borohydride
$CaCO_3$	Calcite
Ag@AuNPs	Bimetallic nanoparticles Ag-core-Au-shell
ELISA	Enzyme-Linked Immunosorbent Assay
min	Minutes
secs	Seconds
SPR	Surface plasmon ressonnce
LSPR	Localized Surface Plasmon Resonance
EF	Enhancement Factor
SILAR	Successive Ionic Layer Absorption and Reaction

XRD	X-ray Diffraction
SEM	Scanning Electron Microscope
EDS	Energy-Dispersive X-ray Spectroscopy
XPS	X-ray Photoelectron Spectroscopy
SERS	Surface Enhanced Raman Spectroscopy
R6G	Rhodamine 6G
LOD	Limit of Detection
PCA	Principal Component Analysis
PC1	Principal Component 1
PC2	Principal Component 2
PBS	Phosphate Buffer Saline

Symbols

I_{SERS}	Raman peak intensity from a certain analyte in an active substrate (SERS intensity)
I_{Raman}	Normal Raman peak intensity from a certain analyte (Raman intensity)
N_{SERS}	Number of molecules responsible for the SERS signal
N_{Raman}	Number of molecules responsible for the Raman signal
I_{Cr}	Crystallinity index

Table of Contents

List of Figures

List of Tables

Motivation

Breast cancer stands out as the most deadliest disease among women around the world. The success rate depends on the early diagnosis, however the available diagnostic methods are not fast enough to guarantee this. Exosomes have been studied as biomarkers, since they participate in the communication between the same cell and different cells, carrying information from the mother cell, and thus can be used as a promising detection tool in the early diagnosis, since this microvesicle are found in almost all body fluids. Current methods of detection of exosomes such as Enzyme-Linked Immunosorbent Assay (ELISA) are not appropriate for an actual diagnostic test due to the need to use samples of very high concentrations and complex preparation.

Optical techniques such as Surface Enhanced Raman spectroscopy (SERS) has shown great interest and sensitivity in this type of tests, besides the need of small sample amounts of reduced concentration, simple preparation and non-destructive. Existing commercial substrates have a high cost and a very short lifetime.

The main objective of this work is the development of a SERS substrate, capable of distinguishing biological samples containing tumoral and non-tumoral exosomes, using paper substrates, in which bimetallic silver-core-gold-shell nanoparticles are directly synthesized in the paper fibers. Rhodamine (6G) will be used as a test molecule for substrate optimization and to verify its SERS sensitivity.

Exosomes from tumoral cells (MDA-MB-231) and non-tumoral cells (MCF-10A) will be isolated, purified and tested with the developed substrates through Raman Spectroscopy. The data will then be analysed through PCA analysis, in order to group these data within 95% confidence ellipses, demonstrating that this can be an important tool in the early diagnosis.

1 Introduction

1.1 Breast cancer exosomes analysis

Every day thousands of people die due to a long illness. In the case of women breast cancer (BCa) it is the most common cause of death worldwide. The disease is more manifested in more developed countries, whereas in developing countries the rates are low but with a tendency to increase[1].

According to Global Cancer Statistics (data from GLOBOCAN 2018), in 2018, almost 2.1 million cases were diagnosed with BCa from which 626,679 women died[2], thus an early diagnosis is very important. Studies had shown that cancers arises due to a series of sequential mutations which occur as a result of genetic instability, environmental factors[3] and other factors like breastfeeding, menopause, oral contraceptives, among others[1].

Nowadays, there are many ways for BCa conventional diagnosis, Mammography is the most common exam used among women around the world, the doctors refute that women over the age of 20 should take this test every year, that consists in a X-Ray picture of the breast. Magnetic Resonance Imaging (MRI), similar to Mammography is also used as a detection method. This method gives a high-resolution image of the breast without the use of harmful radiation. However, for more effective examination the most used is the breast biopsy (tissue sample obtained from the organism for the purpose of examining it in detail[4]) is the most definitive exam for diagnosing all the types of breast cancer[5].

In the past, control of BCa was not possible due to poor knowledge of the molecular mechanisms involved in the pathogenesis of this cancer. Recently, it was concluded that small extracellular vesicles (EVs) named exosomes are involved in BCa development, and for this reason, exosomes can be considered as biomarkers for BCa diagnosis and terapy[6]. Exosomes are small membrane vesicles, (microvesicles), first documented by Pan and Johnstone in 1983[6], with sizes ranging between 30 and 100 nm. These membranes are mostly derived from the fusion of multivesicular bodies with the cell plasma membrane[7], and secreted by normal and diseased cells, during endocytic recycling[8]. It contains genetic information from the cell in which they were formed, mediates cell-to-cell communication by transferring proteins, RNA, and lipids between cells[6,9] and also have autocrine effects on the same cell type contributing to the proliferation of cancerous cells[10] (**Figure 1.1**).

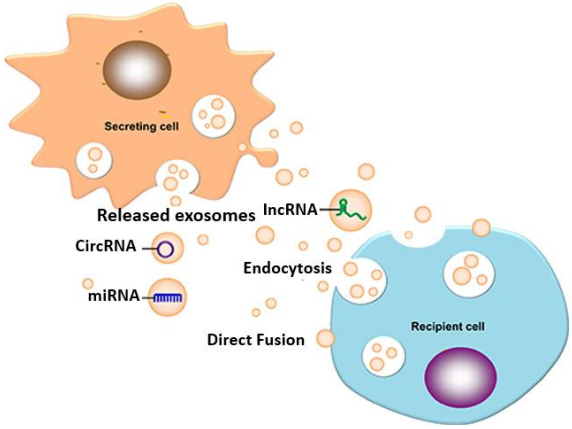

Figure 1.1 - Secretion of exosomes and exosome-mediated transfer. The formation of exosomes starts with the invagination of the plasma membrane, resulting in early endosomes that mature into multivesicular bodies (MVBs). Upon fusion of MVBs with the plasma membrane these vesicles are secreted and release into the

extracellular environment as exosomes, and then they interact with recipient cells. (Adopted from *Jin-Peng Wang et al)*[11]

These small vesicles are of great interest for diagnosis and prognostics applications since they are secreted by cells directly into their local environment and body fluids such as saliva, urine, cerebrospinal fluid, and so on, making them easily acessible[6]. However, EVs from the same mother cell may contain slightly different genetic information making it difficult to detect.[12]

The different methods applied to exosomal detection can be classified into optical and non-optical methods[13]. The non-optical are the most common methods like enzyme-linked immunosorbent assays (ELISA)[8], that allows the detection of specific antibodies presents in the sample, Western Bolt, that separate and classifies the sample proteins based on molecular weight, and thus by type, through gel electrophoresis[14] (despite providing high-resolution molecular information of exosomal content, it requires large amounts of highly concentrated sample, special sample preparation and labelling processes[12,15]) and other methods like X-ray microscope, transmission electron microscopy, atomic force microscopy and impedance-based flow cytometry. As an alternative, there is a need for simpler and faster methods for biological applications, such as optical techniques including scattering flow cytometry (SFC) that relies on the scattered light, Dynamic Light Scattering (DLS), based on measuring the light scattering dependent of the Brownian motion of vesicles and Surface-Enhanced Raman Spectroscopy (SERS), which enhances the electrical field by a surface treatment and analyses vibrational modes of the sample by measuring the non-elastic scattering effect caused by a radiating laser ,among others[8,13].

1.2 Surface-Enhanced Raman Spectroscopy

Nowadays, Raman Spectroscopy is known to be an important method for the evaluation of biological samples, since it gives fingerprint information about the structure and conformation of biomolecules such as proteins, lipids and acid nucleics[16,17]. Thus this analytical technique is capable of providing important information about the biochemical content of exosomes allowing its detection and can be considered a simpler and faster method for biological applications[18].

Raman scattering consists in an inelastic scattering, first characterized by Raman and Krishman in a *Nature* publication in 1928[19]. This phenomenon, known as Raman scattering, is based in the observed change of the wavelength of a photon by molecules rather than an absorption. In other words, the inelastic scattering occurs when some of the energy of the incident photon is lost or increased, in which the frequency changes and equals precisely the difference in vibrational energy levels[20,21]. This excitation energy sets the molecule into a virtual state, the molecule moves to a new state, for a short period of time before the photon is emitted with different energy than the initial frequency of the photon. If the initial energy state is lower than the final state, the scattered photon will be shifted to a lower frequency, ensuring that total energy remains the same (Stokes Shift). In other hand, if the final state is lower in energy, the scattered photon will be shifted to a higher frequency (Anti-stokes shift) (**Figure 1.2**) [22].

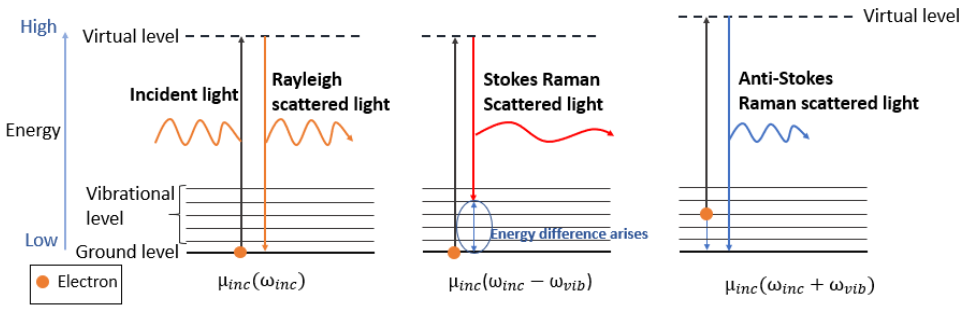

Figure 1.2 - Energy diagram representing (from left to right)- Elastic Rayleigh scattering (left), the inelastic Stokes (middle) and anti-Stokes (right) Raman scattering with ωinc , $\omega inc \pm \omega vib$ and ωvib referring to the frequencies of the incident light, the Raman scattered light, and the molecular vibration, respectively.

Every molecule has its own Raman spectrum, because each functional group have different characteristic vibrational energies [20]. However, one of the major drawback consist on the number of scattered photons related with the vibrational energies within the analyte, 1 in 10^6-10^{10}, causing the Raman signal considerably weak, which places limitations on the detection of analytes at very low concentrations[23]. Other drawback is the strong fluorescence background making difficult to extract the Raman signals[16] being about 14 orders of magnitude smaller than the fluorescence emission in most cases. Therefore, Raman scattering was restricted for many years[20], leading to the need to use high laser power and major time of data collection for spectral acquisition which may lead to degradation of the sample[16].

To solve this problem, Jenmaire and Van Duyne, in 1974, proved that it's possible to greatly enhance the Raman scattering signal placing the scattered near a roughened noble-metal substrate, colloidal solution or roughened electrode [16-20] by noticing that pyridine adsorbed on a roughened silver electrode dramatically increases the Raman signal[24].

This finding allowed the development of Surface Enhanced Raman Spectroscopy (SERS), that greatly improves the Raman signal being strongly enhanced up to 10^{14} times, while suppresses fluorescence emissions at the same time[16].

SERS phenomenon is based on the fact that the local high electric fields are generated when the localized surface plasmon resonance (LSPR) of the metal features on the surface are excited by visible light[22].

There are two enhancement factors that contribute to SERS spectroscopy: chemical (CE) and electromagnetic (EM) enhancement mechanisms. The CE factor is usually associated with the transferring of charges between the adsorbed analytes and metal nanofeatures on the surface. The EM is the dominant contribution, where there is an increase of the electromagnetic field caused by the interaction of the light on the metal surface inducing the excitation of the plasmon.[17]

1.2.1 Chemical enhancement effect

This effect consists on a transfer of charge between the metal structure and the absorbed molecules. The charge transfer possible to occur it's about half the energy of the intrinsic intramolecular excitations when the energy of highest occupied molecular orbital (HOMO) and lowest unoccupied molecular orbital (LUMO) of the adsorbate are distributed according to the Fermi level of the metal[25]. The existence of this charge-transfer sate leads on a major probability of Raman transition by providing a pathway for resonant excitation. This mechanism strongly depends on the direct interaction between the substrate and the adsorbate, being limited by the first adsorbed molecules, resulting on smaller enhancement compared to the EM[21].

1.2.2 Electromagnetic enhancement effect

As described above, EM effect consists on the interaction of an electromagnetic wave with a metal surface, typically composed of gold (Au) and/or silver (Ag)[22]. These metallic nanoparticles (MNPs) have been a subject of research for decades due their associated strong plasmon resonance frequency (delocalized conduction electrons- named *plasmas oscilatiors*)[20] which represents an enormous interest in areas such as nanoscale photonics and biological sensing[26]. This surface plasmon resonance varies depending on the NPs properties such as metal type, size, shape, distance between particles and also the dielectric environment of the MNPs[26].

The enhancement results from the amplification of the light by the excitation of localized surface plasmon resonances (LSPRs)[27], leading to a local enhance electromagnetic fields due the fact that particle surface plasmon resonance allows direct coupling of light to resonant collective electron plasmon oscillation (**Figure 1.3**). A Coulombic attraction appears, acting as a restoring force between negatively charged electronic cloud with a positively charged metal surface. Those wavelengths of the incident light that equals to this resonance frequency are absorbed and can be elastically re-emitted as scattered light from nanoparticles, acting as an antena[22].

Therefore is important to obtain a rough surface because of this light concentration that occurs preferentially in the gaps, crevices or sharp features of plasmonic materials.[26]

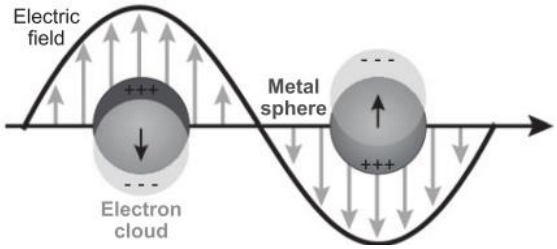

Figure 1.3 - Illustration of LSPR phenomenon

1.2.3 SERS Enhancement Factor and hot spots

Due to an increase of local electric field on SERS substrates, an increase in the signal strength is observed, comparatively with the Raman scattering, and the enhancement factor (EF) is a measure of the efficiency of SERS substrates. The constant development of new SERS substrates creates the need to compare them with each other, already known in the literature[28], knowing that the single molecular (SM) detection is one of the main objectives in the development of SERS substrates. EF is a quantitative method to express this capacity, with values above 10^8-10^{10} are, in fact, sufficient for the detection of SM-SERS.[28] The average EF shall be calculated from the following equation:

$$EF = \frac{I_{SERS}}{I_{Raman}} \times \frac{N_{Raman}}{N_{SERS}} \quad (1.1)$$

Equation (1.1), describes the average Raman enhancement and the enhancement of the incident wavelength and the resulting Stokes-shifted Raman field[22], where I_{SERS} and I_{Raman} are the scattering intensities of the SERS and normal Raman substrates, and N_{SERS} and N_{Raman} are related to the number of molecules that contribute to the inelastic scattering evaluated by SERS and normal Raman scattering measurements[29].

Although it is hard to produce substrates that consistently provide enhancements for single molecule detection. The effort to improve EF has led to a tremendous interest in the properties of nanoparticles. Metal aggregations, nanoparticles different shapes, for example, pointed edges, like star shapes, or conjugation of different nanoparticles such as bimetallic, creates punctual locations called “hot-spots”, in which near-field intensities are greater than the far field intensities when under resonance conditions and consequently the increase of the signal intensity. Studies

are underway to ascertain the influence of sizes, shapes of nanoparticles and interparticle distances, smaller than 2 nm induce extraordinary enhancements on SERS phenomena due to the generation of nonlocal effects and quantum confinement [25,30,31,32].

1.3 Bimetallic nanoparticles on SERS application

For SERS are commonly used all types of metallic features in all kind of shapes and sizes, like sphere or star-shaped nanoparticles. Metallic nanoparticles have their strong plasmon resonance which is used for enhancement proposes in fields such as nanoscale photonics and biological sensing[26]. Silver and gold nanoparticles (AgNPs and AuNPs, respectively) are the most common metallic compounds used for SERS implementation due to their unique optical, electric, magnetic and catalytic properties[33]. Despite offering a strong surface plasmon resonance effect, AgNPs suffers a rapid decrease in SERS efficiency due to state of early oxidation. On other hand, AuNPs are more stable nanoparticles than AgNPs, however provides a considerably decrease in SERS efficiency in terms of detection of a single molecule[28]. In addition, the use of gold is also advantageous for the detection of exosomes, since it's been used on experiments with biological compounds and shows an incredible biocompatibility[34,35]. Bimetallic composite nanoparticles composed of two different metal elements structures have shown a great interest for this type of applications than monometallic nanoparticles. The bimetallic nanostructures are defined by the distribution and orientation of the elements. This structures can be oriented randomly alloy, alloy with an intermetallic compound, cluster-in-cluster and core-shell structures.[36] This work is based on bimetallic nanoparticles (Ag@AuNPs) core-shell structure in order to increase the SERS EF and overcome silver oxidation[28].

1.3.1 Solid surface matrix and Ag@AuNPs SILAR-synthesised

A SERS substrate consists in a nanofabrication of metallic features, taking into account that the substrate used in SERS has as main and fundamental requirement to support the LSPR capable of providing the greatest amount of "hot-spots" in order to achieve great enhancements[21,22] for on-site applications.

Cellulose substrates have been widely used for SERS due to its flexibility, lightweight, low-price and user friendly, requirements for a substrate to be used as sensing support for on-site applications [22]. Cellulose matrices such as paper are also used to increase substrate rugosity due to the random orientation and texture of their fibers, thus increasing the number of "hot-spots". Dipping and printing the paper strip for deposition of plasmonic nanoparticles are techniques that have been studied, however they have shown a non-uniform distribution of SERS-active region. Apart from that, these methods require complicated processes[28]. In this project, it was used a recent technique of deposition of Ag-Core-Au-Shell nanoparticles (Ag@AuNPs) directly on the paper substrate based on layer-by-layer deposition of opposite charges (positive and negative ions), called SILAR (Successive Ionic Layer Absorption and Reaction). The SILAR method was firstly introduced by Nicolau in the 80s as a technique for thin films depositions[37]. SILAR is mainly based on the adsorption and reaction of the ions and solvated ions on the solid-liquid interface. It is separated in 2 stages, the first stage consists in the formation of AgNPs (core) and the second stage translates into the synthesis of AuNPs (shell) over the already synthesized AgNPs. In both stages, metal cations (Ag^+ and Au^{3+}) are adsorbed onto the paper. The next step consists of washing the paper with deionized water (DW) in order to eliminate all the excess unadsorbed cations. Next, the paper is immersed on the reducing solution ($NaBH_4$), allowing the reaction to occur. The adsorbed cations in contact with the sodium borohydride ions (BH_4^-) reacts and a solid adsorbed compound is formed on the surface. Again, the substrate is washed with

water to expel the ions in the diffusion layer weakly bonded to the paper fibbers (**Figure 1.4**). It is expected to obtain raspberry-shape nanoparticles. The need of low deposition temperatures, easy to performed and control the size of nanoparticles through multiple repetitions of chemical reactions are characteristics that make this technique quite appealing[28].

Figure 1.4 Scheme of the two-stage SILAR fabrication of the Ag@AuNPs core-shell on the cellulose substrate (Adopted from *Wansun Kim et al* [28]).

2 Materials and Methods

2.1 Production technique of the paper bimetallic features Ag@AuNPs by two-stage SILAR fabrication procedures on the cellulose substrate.

The synthesis performed in this work were based on the two-stage SILAR[28] method where the bimetallic nanoparticles were directly synthesized on the paper by the successive ionic layer absorption and reaction.

Two types of paper were used as substrate: Whatman nr. 1 (Whatman Internacional Ltd., Florham Park, NJ) and Office paper (300%, Portucel Soporcel, Setúbal, Portugal).

SILAR process

All the glass material was immersed with aqua regia for at least 5 hours, to ensure that all the particles were eliminated. Next all the material was placed under running water and its pH value was checked and washed again with Milli-Q water, until a pH of 7.0.

The SILAR synthesis was performed according to the schematic representation depicted in **Figure 2.1**.

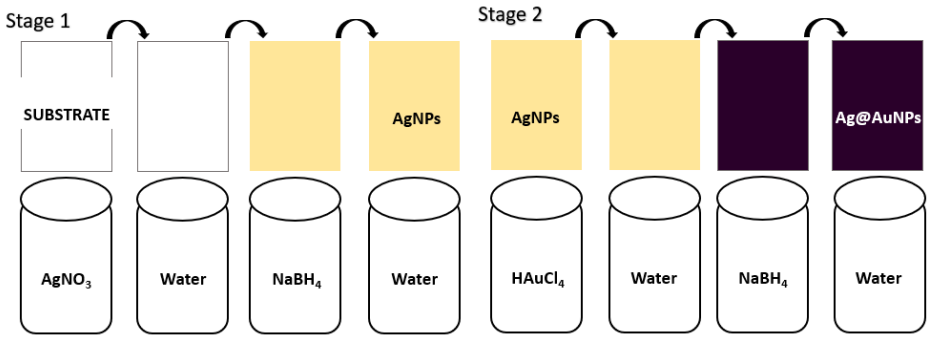

Figure 2.1 - Scheme of two stage SILAR technique. Representation of stage 1 and stage 2 of the process.

- With reducing agent:

An optimization on the concentrations of reactants and number of cycles was perform along this work. The protocol detailed below shows the optimized conditions.

Firstly, the AgNPs-core (**Figure 2.1**, **Stage 1**) was directly synthesized on the paper strip, using 6 cycles with 20/20 mM of $AgNO_3$/$NaBH_4$: the paper substrate was dipped in aqueous silver nitrate ($AgNO_3$>99%, from Sigma-Aldrich) and washed with Milli-Q water. Then it was dipped in the reducing agent solution of sodium borohydride ($NaBH_4$>96%, from MERCK) and rinsed with Milii-Q water to remove all the residual non-reactants. Stage 2 consists on the synthesis of the AuNPs-shell (**Figure 2.1**, **Stage 2**) using 2 cycles with 1/1 mM of $HauCl_4$/ $NaBH_4$): the paper with AgNPs already synthesized, was dipped in an aqueous solution of gold (III) chloride trihydrate (HauCl4>99%, form ACROSORGANICS) and rinsed with Milli-Q water. Then it was treated in $NaBH_4$ reducing solution and rinsed once again with Milli-Q water. In the SILAR fabrication, one cycle includes four successive steps such as the treatment of the substrate in a metal salt solution ($AgNO_3$ or $HAuCl_4$) and rinsed to wash out non-reacted remains, re-treatment of the paper in the reducing solution and again washed with water. Each step has a duration of 30 sec, making 2 min the total time of a cycle.

- Without reducing agent on stage 1.

Unlike the SILAR method described above, for the office paper no reducing agent was used. The AgNPs-core were grown directly on the substrate, according to the experiments (8 cycles with 20 mM of $AgNO_3$). The paper strip was sunken in aqueous silver nitrate and washed with Milli-Q water, counting as a cycle in order to remove all the non-reactants, the time of each step was increased to 40 sec in agreement with the newly optimized conditions. Secondly, the AuNPs-shell were deposited directly into the AgNPs-core in accordance with **Figure 2.1- stage 2**, keeping the time of each step following the already optimized conditions[28].

2.2 Exosomes growth and isolation

The isolation of exosomes was performed at Champalimaud Foundation (CF), where all the equipment and materials were made available for the cell culture of tumoral (MDA-MB-231) and non-tumoral (MCF-10A) exosomes and its isolation.

2.2.1 Cell culture

For the growth of the tumoral cells (MDA231-TGL), it was prepared a culture medium by adding to a 500 ml of DNEM (Lonza™ BioWhittaker™), 1% of Penicillin/Streptomycin (P/S) antibiotic solution to prevent contamination of exosomes and 10% of Fetal Bovine Serum (FBS, from Biomest). Both reagents were frozen and heated to 37°C to prevent thermal shock of the cells. Then an Exo-free medium was prepared: 40 ml of FBS was ultra-centrifuge (*Beckman Coultier*, Optima XPN-100 Ultracentrifuge) at 100000 xg, for 2h20min at 10°C, using a 45Ti motor, and passed through a filter to discard all the obtained pellet, and a new culture medium was prepared with the same reagents and the same proportions described above, with the Exo-free PBS.

After the cells are thawed, 1 ml were added to 8 ml of culture medium (DNEM+FBS+P/S) in order to remove the remain Dimethyl sulfoxide (DMSO), followed by centrifugation at 1200 rpm for 5 min at 24°C (*Sorvall*, ST40R, centrifuge). After removing the supernatant, the cells were re-suspended with 20 ml of culture medium then leave to incubate at 37 °C with 5% of CO_2 in a 175 ml culture flask. Once reached the confluence point, the number of cells were estimated using a haemocytometer to guarantee the existence of 1 million cells per ml and then distributed by 5 culture dishes (1 ml of cells and 19 ml of Exo-free culture medium) and was left to incubate for 2 days at 37 °C with 5% of CO2 until reaching the confluence point.

The cell passages were made by sucking the culture medium, with a small vacuum system, then the phosphate buffer saline (PBS 1X 7.4 pH, Lonza) was added in enough quantity to cover the bottom of the flask and the same amount of trypsin to detach the cells from the bottom and leave to incubate for 5 min. Then 10 ml of culture medium was added to neutralize the trypsin and centrifuged at 1200 rpm, for 5 min at 24 °C.

For non-tumoral cells, the procedure was the same described above with few exceptions. The Dulbecco's Modified Eagle Medium/Nutrient Mixture F-12 (DMEM/F12, Sigma-Aldrich) medium was supplemented with 5% of Horse Serum and Epidermal Growth Factor (EGF, 20 ng/ml), Hydrocortisone (0.5 mg/ml) and Cholera toxin (100 ng/ml) and due to a toxicity of this toxin, this process was done on the biosafety unit BSL2 of the CF.

2.2.2 Exosome Isolation/purification and labeling

The process of isolation and purification was the same for both cellular lines. First, was collected the culture medium and then centrifuged at 500 rpm for 10 min at 10 °C to remove all dead cells and remain only the medium rich in exosomes. Then a second centrifugation was performed after removal of the previous pellet at 3000 g for 20 min at 10°C and storage at 80°C.

The collected supernatant was then transferred to an ultracentrifuge tube and two ultra-centrifugations were performed at 12000 xg for 2h20min at 10 °C and discarding the pellet. The resulting supernatant was submitted to another centrifugation at 100 000 xg for 2h20min at 10 °C and finally discarded, obtaining an aggregated pellet containing the exosomes. Then, the purification process is followed with the sucrose cushion. To a 4 ml sucrose solution (protocol in **Appendix B, B1**) was slowly added 14 ml of PBS diluted with the previously obtained pellet, to not break the sucrose layer and proceeded to ultra-centrifugation at 100 000 xg for 1h10min at 10 °C. Then, about 5 ml of the resulting phase mixture of sucrose and exosomes was collected far from the pellet. Finally, 16 ml of PBS was added to the collected fraction and the last ultra-centrifugation was carried out overnight at 100 000 xg at 10 °C, and the resulting pellet was resuspended in 100 – 200 µl of PBS.

2.3 Characterization techniques

2.3.1 Characterization of SILAR-synthesized Ag@AuNPs

Different papers (Whatman n. 1 and Office): The papers were morphological analyzed through Scanning Electron Microscopy (SEM, *Carl Zeiss AURIGA FIB-SEM Croossbeam*), to investigate and compare the type and density of paper fibers. Energy Dispersive X-ray spectroscopy (EDS) coupled with SEM imaging was used for chemical identification of the paper fibers. The conductive coating (Iridium) on the paper samples was performed by sputtering (Quorum).

X-ray Diffraction (XRD, *PANalytical, X'Pert Pro*) was done to have a structural analysis and subsequent calculation of the crystallinity index.

SILAR-synthesized Ag@AuNPs: The obtained composites were also morphologically characterized by SEM and EDS, as described above, with the exception that for EDS analysis Iridium was not used to avoid gold peak overlap with the iridium peak, instead carbon was used.

X-ray photoelectron spectroscopy (XPS, *Kratos, Axis Supra*) was used for superficial chemical identification to confer the presence of metallic features of silver and gold. X-Ray Diffraction (XRD) was used for diffractogram obtainment to check for cellulose, silver and gold diffraction peaks.

The SILAR-synthetized papers were tested as SERS substrates using *Renishaw® inVia™ Qontor®* confocal Raman microscope and using both lasers (532 and 633 nm) depending on the purpose of the measurement. The Raman Shift wavenumber scan was centred at 1200 cm^{-1}.

The baseline was subtracted from all spectra using the WiRE™ 5.0 software.

Tumoral and non-tumoral exosomes: The *NanoSight®*, NS300, located at Champalimaud Foundation, was used to characterize the size distribution of isolated and purified exosomes from both cultured cellular lines (tumoral and non-tumoral). The samples were diluted 1:3000 and 1:5000 for tumoral and non-tumoral exosomes, respectively. Results are presented in **Appendix B, B2**.

3 Results and Discussion

The main purpose of this work was the development of new, efficient, cheap, flexible and environment-friendly substrates for SERS applications. For that, it was studied two types of cellulose substrates: Whatman no.1 and Office paper. The obtained substrates were morphologic and chemically characterized by the techniques described in the previous chapter and finally tested as SERS active substrates.

3.1 Characterization of cellulose base support: Whatman no.1 and Office paper

Both papers were morphologically characterized, by SEM, in order to understand and compare the type and density of the fibers.

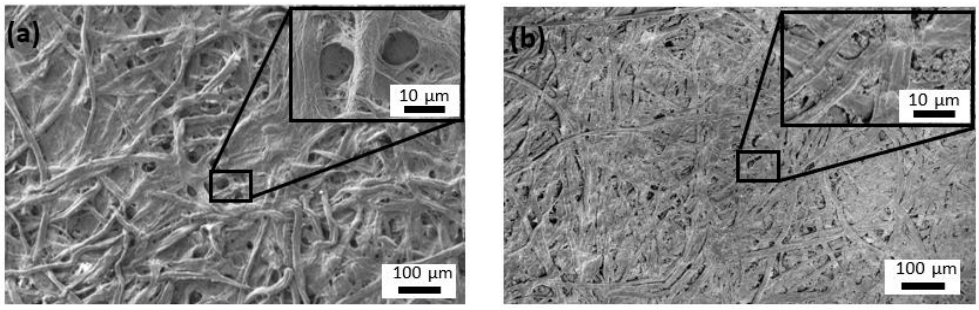

Figure 3.1 - SEM images of Whatman no.1 fibres (a) and Office paper fibres (b)

It is crucial for SERS that the nanoparticles concentrate on the surface to interact as much as possible with the analyte to achieve higher signal efficiency[22]. In the figure above it's possible to observe at microscopic level the random arrangement of fibres on both papers. The Whatman (a) paper fibres have a more cylindrical geometry, which contributes to a larger paper thickness, unlike Office paper (b) which has flatter fibres. Whatman is a lot more porous than the Office paper, and the latter seems to have a higher fibre density indicating that this one has a flatter surface.

Besides that, it's possible to observe that the Office paper is covered by calcium carbonate ($CaCO_3$) crystals resulting from the bleaching process that the paper undergoes (a process that chemically modifies the materials themselves)[38]. The presence of this salt was suspected to aid in the formation of NPs.

The average fiber and pore diameter of the papers were calculated using ImageJ software and the results are shown in **Table 3.1**.

Table 3.1 - Values of fibre diameter, porosity and pore size of Whatman and Office paper

Paper type	Fiber Diameter (µm)	Porosity (area %)	Pore diameter (average)
Whatman	15.04±3.05	36.82	24.80±7.50
Office	13.06±4.10	17.60	11.10±4.28

The obtained results show that in terms of fiber diameter, the two papers are very similar. However, the office paper, as is well visible in **Table 3.1**, has a significantly lower porosity and

pore size, indicating that the surface area of office paper is higher than Whatman paper, although office paper pores are mostly covered by the salt

In addition, SEM-EDS was used. It's an important technique to perceive the differences between substrates, since this is a semi-quantitative analysis giving information on the chemical composition of the sample, it's possible to confirm not only the existence of certain elements, but also their relative quantity[39]. In both papers, the prominent peaks, represented in the spectrum of **Figure 3.2**, correspond to Carbon, C (E = 0.28 keV), and Oxygen, O (E = 0.52 keV) since these are the constituents of cellulose, the main component of paper. Also, the common initial peak to all papers, corresponding to (E = 0 keV), is characteristic of the equipment and the Ir peaks at E = 1.98 keV and E = 2.08 keV are related to the paper coating (thickness of 10 nm) and not to its composition.

Comparing to Whatman no.1 paper (98 % of cellulose), office paper is composed by more elements[40]. The presence of the $CaCO_3$ salt in office paper is confirmed by the detection of Calcium (Ca) (E = 3.7 keV and E = 4.02 keV). Also, other elements were detected in residual quantities such as Sodium (Na) (E = 1.04 keV), Silicon (Si) (E = 1.48 keV) and Chlorine (Cl) (2.62 keV). The Si is the main constituent of the support used in this technique and the remaining elements are possible contaminations of the papers.

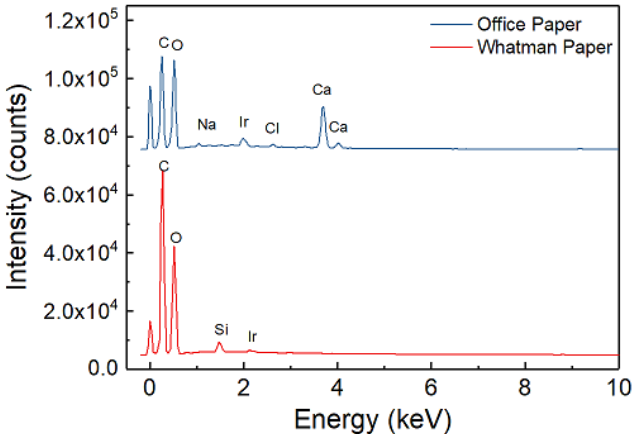

Figure 3.2 - EDS analysis of the paper substrates. Cumulative spectra of the EDS analysis of the Whatman no.1 paper (red) and office paper (blue). The chemical symbols on the top of each peak represent the corresponding element identified by the EDS technique and the intensity is indicative of the relative quantity of the elements.

In addition to the cumulative spectrum, the EDS analysis also provides a distribution map of the different types of detected elements (**Appendix A, Figure A1**). The distribution maps confirm that oxygen and carbon are the main constituents of the cellulose fibers of both papers. Calcium is only possible to observe on office paper, as expected, and is in a considerable proportion in relation to carbon and oxygen and according to the map of distribution this element is in the form of agglomerate between the cellulose fibers.

In complementarity the structural analysis of the papers was made through X-ray diffraction and the diffractograms are represented in **Figure 3.3,** also indicating the identified crystalline structures.

It is possible to observe that the papers show the crystalline diffraction pattern of type I cellulose with the main peaks at 14.9º, 16.6º and 22.8º in 2θ values, corresponding to the crystalline planes ($11^{-}0$), (110) and (002), respectively[41]. However, the office paper presents the

two first peaks convoluted at 15.9º, indicating the presence of amorphous components in its structure, such as hemicellulose and lignin[42].

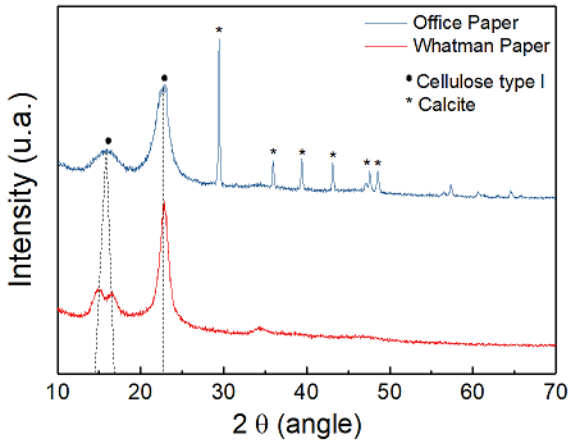

Figure 3.3 - Diffractograms of office (blue) and Whatman paper (red). The peaks corresponding to Cellulose type I and Calcite ($CaCO_3$) are represented.

By this technique it is also possible to determine the index of crystallinity (I_{cr}) of the substrates which can be calculated using the maximum intensity of the plane (002) of the crystal structure of type I cellulose, $I_{(200)}$, (peak at 22.8 °) and the intensity of the $(11^{-}0)$ plane peak, related to the amorphous components of the cellulose, $I(11^{-}0)$, using the Segal empirical method, through **Equation 3.1**:

$$I_{Cr} = \frac{I_{(002)} - I_{(11^{-}0)}}{I_{(002)}} \times 100 \qquad (3.1)$$

As expected, office paper has a lower index of crystallinity (69 %) than Whatman paper (74 %), confirming what was previously said.

In addition, the analysis of the office paper diffractogram identifies the crystalline form of calcite, showing peaks around 29.4º, 35.9º, 39.4º, 43.1º, 47.5º and 48.6º that aren't present in Whatman paper. These peaks were related to the (104), (110), (113), (202), (018) and $(11\bar{6})$ crystal planes, respectively. Calcite ($CaCO_3$) represents 20% of the office paper composition and is the main additive used in the photochromic papermaking process. It forms porous agglomerates that impart opacity and brightness, altering the optical properties of the paper[41–43].

3.2 SILAR-synthesized Ag@AuNPs

In this work, a method of successive adsorption and ion-layer reaction (SILAR) was used for the formation of bimetallic nanostructures of gold and silver directly on the substrates (Whatman and office paper). This is a simple and inexpensive method, done at room temperature and requires less synthesis time compared to conventional methods such as Chemical Vapor Deposition (CVD), Metal-Organic Chemical Vapor Deposition (MOCVD), among others, that are very cumbersome and inefficient for the deposition of complex materials[44]. The synthesis is based on treating the substrate separately with each aqueous precursor solution so that the adsorption and reaction can occur.

The core@shell nanoparticles are constructed by two-stage SILAR fabrication procedures including the formation of AgNPs (core) into paper and the synthesis of AuNPs (shell) on the AgNPs. The first stage consists on AgNPs synthesis, the silver cations (Ag^{+}) are adsorbed onto

the paper, and then all the excess unadsorbed cations are washed away by rising the substrate with purified water. The rinsing is followed by the reaction step where the paper is dipped into the aqueous anion precursor solution ($NaBH_4$) and the solvated anions (BH_4^-) react with the adsorbed cations forming a solid Silver compound (Ag^0) on the surface and once again the unadsorbed ions are washed away with purified water. The second stage consists on AuNPs synthesis over the AgNPs already formed. First, the paper is immersed into an aqueous solution of $HAuCl_4 \cdot 3H_2O$ and the gold cations (Au^{3+}) are adsorbed onto the paper and the excess unadsorbed ions are washed away with deionized water. Then the paper is immersed in the reducing solution where the reaction takes place, the anions (BH_4^-), in the diffusion layer, react with the adsorbed cations forming a solid Gold compound (Au^0) over the Silver. By repeating these deposition cycles, nanoparticles can be formed layer by layer. The size of the nanoparticles and their growing shape is controlled by the number of deposition cycles.

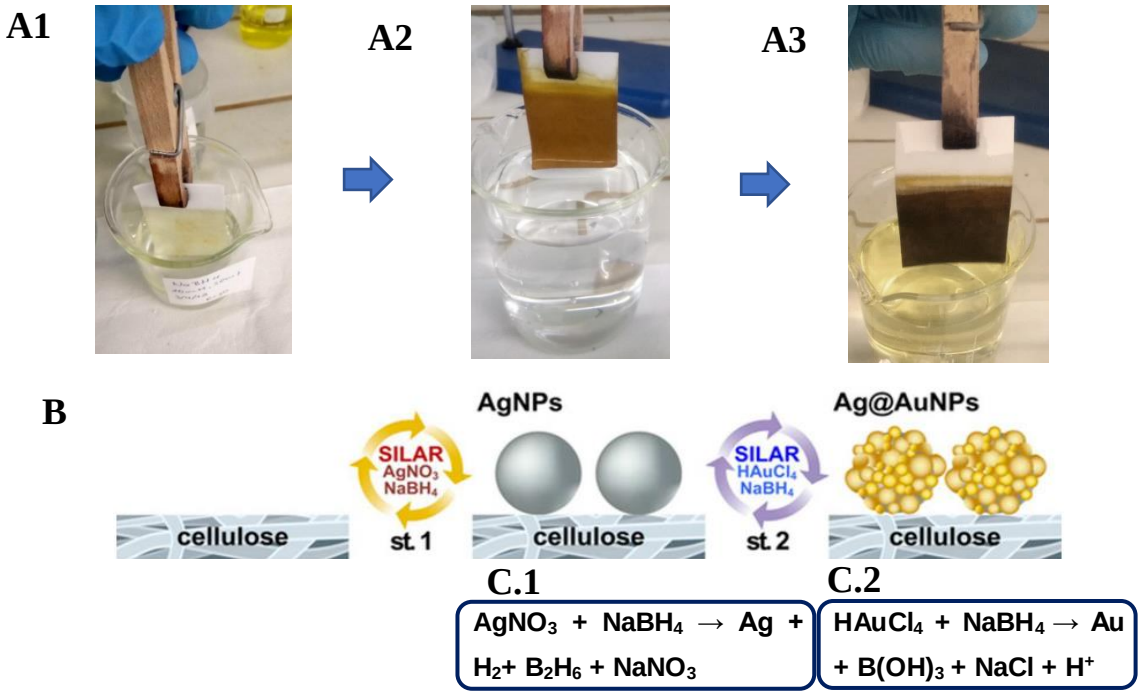

Figure 3.4 The images A1, A2, A3 correspond to what was actually done in SILAR-synthesis, where the papers are immersed in the solutions of each SILAR-cycle. A1-Beginning of the SILAR cycle for the formation of AgNPs, A2- end of SILAR-synthesis cycles for the AgNPs formation, A3- end of the synthesis cycles for AuNPs formation. B- Scheme of the two-stage SILAR fabrication procedures of Ag@AuNPs on the cellulose substrate (Adopted from *Wansun Kim et al* [28]). C1 and C2 correspond to the chemical equations equivalent to reactions in the paper fibers when the nanoparticles are synthesized.

3.2.1 Optimization of SILAR-synthesized Ag@AuNPs on Whatman paper no 1

At first, the Ag core were synthesized directly on the paper strip, according to the previous optimized SILAR conditions- 6 cycles of 20/20 mM of $AgNO_3/NaBH_4$[28]- as this is a method of ionic adsorption and reaction, by increasing the number of SILAR cycles performed will also increase the diameter of the formed AgNPs until they fuse and form a thin film of silver[45].

The same phenomenon happens during Au shell formation, ionically deposited in the AgNPs core. In previous studies have shown an optimized SILAR conditions and concentrations of 6

cycles of 10/10 mM of $HAuCl_4/NaBH_4$, which in fact increased SERS efficiency by increasing the number of cycles (**Appendix C, Figure C1**). However, comparing the bimetallic nanoparticles to the Ag monometallic ones, the latter presents a superior SERS effect, showing that this effect was likely to be induced by only gold nanostructure rather than bimetallic nanostructure possibly due to the AuNPs diameter could be twice as large as AgNPs, even though the concentration of $HAuCl_4$ ions (10 mM) is half the concentration of $AgNO_3$ ions (20 mM)[28]. So, a new SILAR concentration was chosen, 1/1 mM of $HAuCl_4/NaBH_4$, in order to minimize the influence of gold and prevent the silver from being completely covered by gold nanofeatures (**Figure 3.5**).

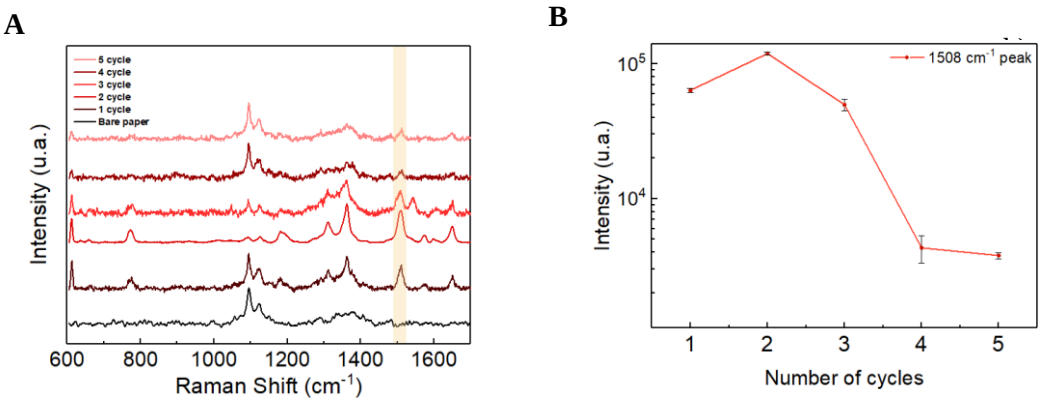

Figure 3.5 - Raman spectra and (B) intensities of 1 mM R6G characterized peak at 1508 cm^{-1} with the number of SILAR cycles for decorating the shell AuNPs on the core AgNPs. The number of cycles and their intensities is plotted on the log scale because the intensity values of 4 to 5 cycles are very close to zero.

A droplet of 10^{-6} M of Rhodamine (R6G) molecule was used to evaluate the SERS activity, since this is a widely studied dye in this area, easy to interpret and presents well defined characteristic peaks. The characteristic peak of R6G chosen for the study was 1508 cm^{-1} instead of 1363 cm^{-1}, although the latter shows higher intensities, also presents a greater contribution of the cellulose, which may inference with the measurements. The same conditions were used in all measurements (15 secs of exposure time, 5% of laser power and 5 accumulations), in order to guarantee a reliable comparison (**Figure 3.5**). Also, the 633 nm laser was used due to being closer to the gold SPR peak, resulting in higher plasmonic activity. Although the substrate contains silver and gold, when using the 532 nm laser, fluorescence phenomenon was verified, often resulting in signal saturation. The Raman peak of R6G continued to increase until two SILAR cycles, then it decreases slightly until the 3 cycles and greatly decreased for 4 and 5 cycles (**Figure 3.5-B**). Which is in agreement with the findings already made, with the increase of the number of gold SILAR-cycles, the particle size will also increase, eventually covering the entire silver core and the Ag cease to be the major contributor to the signal. The two SILAR cycles were selected as an optimal condition for decorating the shell AuNPs on the core AgNPs.

As an outcome, the bimetallic nanoparticles (Ag@AuNPs) produced by the SILAR process compared to the monometallic ones (AgNPs and AuNPs) produced by the same method demonstrate an incredible SERS effect (**Figure 3.6-A**). The substrates were maintained under the same laboratory conditions (away from light and kept in the fridge) and tested 30 days after the synthesis. The SERS activity of AgNPs paper showed a 75% degradation (assessment based on peak area and intensity under investigation), while that of Ag@AuNPs paper showed less than 10% degradation (**Figure 3.6-B**), indicating that the AgNPs suffered a greater oxidation, thus

proving the stabilizing power of the gold over the bimetallic nanoparticles, leading to a moderate anti-oxidation effect.

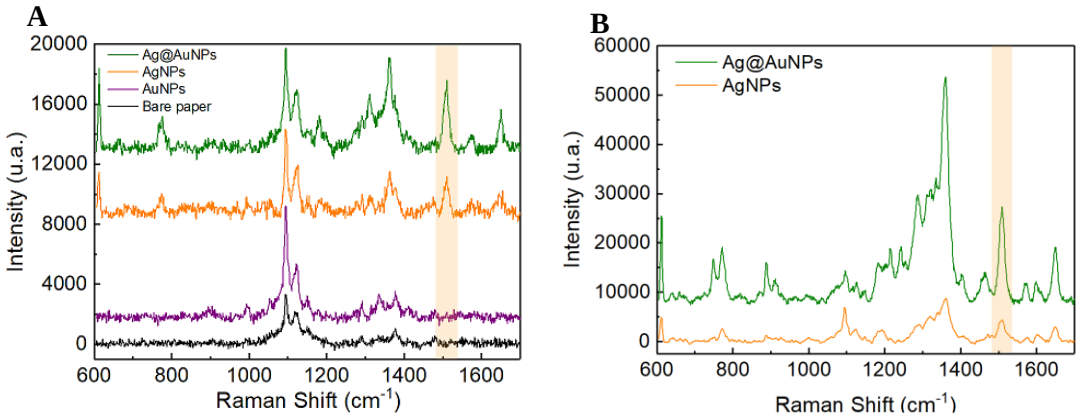

Figure 3.6 - Raman spectra of 10^{-6} M R6G with bare paper and AgNPs, AuNPs and Ag@AuNPs on paper right after the synthesis; (B) Raman spectra of 10^{-6} M with Ag@AuNPs and AgNPs on paper 30 days after the synthesis.

Once synthesis is optimized in Whatman paper, it was tested the sensitivity of the substrate containing bimetallic nanoparticles. Small squares of the substrate were cut with 5 x 5 mm each side, 2 µl of R6G was used and 3 points were randomly chosen for data collection. The mean spectra is represented in the **Figure 3.6**. Different R6G concentrations were tested, the highest of 10^{-6} and the lowest of 10^{-12} M, the peak intensity rapidly decrease with the lowering of the R6G concentration, showing that the limit of detection (LOD) achieved was 10^{-11} M (**Figure 3.7**), contrary to what was reported by *Wansun Kim, et. al*[28] which his team was able to detect concentrations of 10^{-15} M. The peaks associated with 10^{-8} M and 10^{-9} M (Left) are smaller than expected and may be associated with the degradation of these solutions.

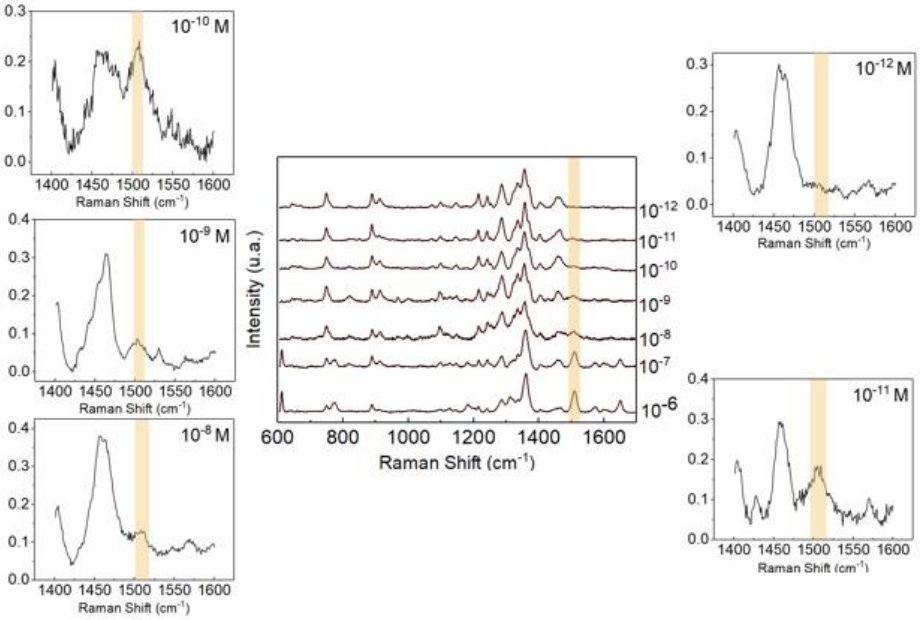

Figure 3.7 - Three measurement average of rhodamine SERS spectra on the optimized SILAR-synthesised Ag@AuNPs whatman nº1 substrate with different concentrations. (Left) zoom of the 1508 cm^{-1} peak range for 10^{-8} M, 10^{-9} M and 10^{-10} M. (Right) zoom of the 1508 cm^{-1} peak range for 10^{-11} M and 10^{-12} M.

The enhancement factor (EF) was calculated using the equation (1.1). For this, spectra were compared using different R6G concentrations: 10^{-2} M measured on a glass and 10^{-6} M measured on the substrate. (**Appendix C Figure C2**). N_{RAMAN} and N_{SERS} were substituted for the R6G concentrations: 10^{-2} and 10^{-6} M, respectively. I_{RAMAN} and I_{SERS} were replaced by the peak area corresponding to the 1508 cm^{-1} band, measured on the glass and on the optimized substrate, respectively. The peak area was used to obtain a more real EF value. The obtained EF was 3.5×10^4.

As the optimized substrate found, homogeneity tests were performed with R6G 10^{-6} M. Twenty measurements were made between the same substrate and different samples of the same substrate at random points, also the measurement conditions were kept and the results are presented in **Figure 3.8**.

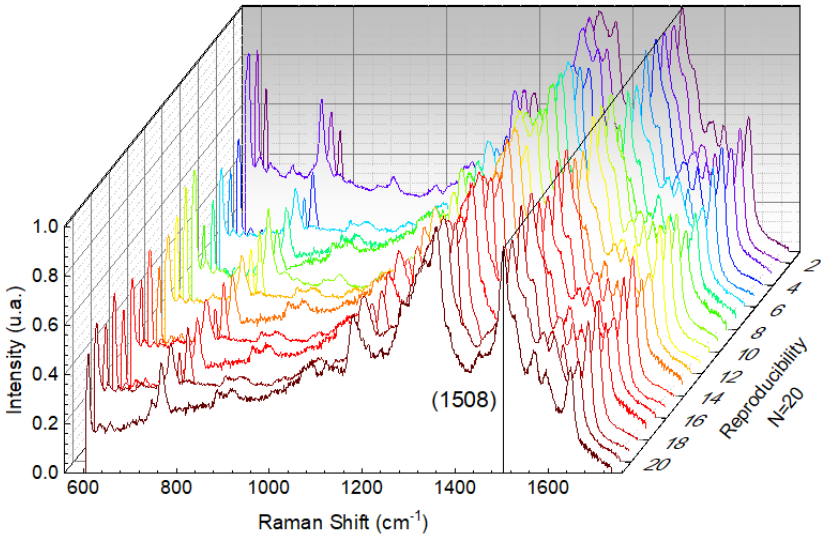

Figure 3.8 - Homogeneity tests of Whatman n.1 SERS substrate with Ag@AuNPs.

The line indicates the peak under study (1508 cm^{-1}). Although not very consistent, at almost all points the spectrum obtained shows well-defined peaks while the intensity is not constant indicating that the paper may not be evenly coated with nanoparticles.

3.2.2 Optimization of SILAR-synthesized Ag@AuNPs on office paper

The same SILAR-synthesis tested inWhatman nº1 was also tested in the office paper. The EF obtained was found to be 9.2×10^4, higher than that obtained with whatman paper, while the limit of detection (LOD) remained the same, 10^{-11} M. In this office substrate with Ag@AuNPs SILAR-synthesized, biological tests were performed between tumoral exosomes and PBS (control) and tested with PCA, which was not effective because the of the 95% confidence ellipses overlapped. It was concluded, that this poor result was due to the great contribution of the cellulose that overlapped the characteristic peaks of the biological samples, leading to the need to create a substrate, with more NPs on the surface, increasing its SERS efficiency and decrease of cellulose contribution.

Other synthesis conditions were tested on this paper. Since this is a synthesis of successive ionic layer adsorption and reaction which is a layer-by-layer deposition of oppositely charged, positive and negative, ions of two salts: metal salt ($AgNO_3$ and $HAuCL_4$) and reducing salt ($NaBH_4$). Since the office paper has $CaCO_3$ in its fibers, it was tested the reducing power of this

salt in the formation of silver nanoparticles, since the AgNPs provided a superior SERS efficiency compared to gold, the focus was to modify the silver synthesis conditions on office paper to get more nanoparticles to contribute to the SERS signal and at the same time have a greener and environmentally friendly synthesis, due to the absence of $NaBH_4$ as reducing agent.

In the already optimized SILAR fabrication, one cycle included four steps: treatment of the substrate in a metal salt solution ($AgNO_3$); washed with water to remove unreacted elements; re-treatment of the paper in the solution with the reducing agent; washed with water again. Each step lasts 30 secs, making 2 min per cycle and a total of 6 cycles. The reducing salt $NaBH_4$ was removed from the equation and the paper was only treated with the silver salt solution, expecting that the reaction between $AgNO_3$ and $CaCO_3$ to occur during the cycle, reducing the time of each cycle in 30 secs, but maintaining the number of 6 cycles. In order to evaluate the effectiveness of the synthesis, 10^{-6} M of R6G was used and the characteristic peak of rhodamine was analysed at 1508 cm^{-1}. The laser used in these measurements remained at 633 nm which demonstrated a smoother spectrum with less noise. The measurement conditions were 10 secs of exposure time, 1% laser power (higher showed signal saturation and lower showed more noise) and 10 accumulations. 3 random spots were chosen for the measurements and the average spectra is represented in the **Figure 3.9.**

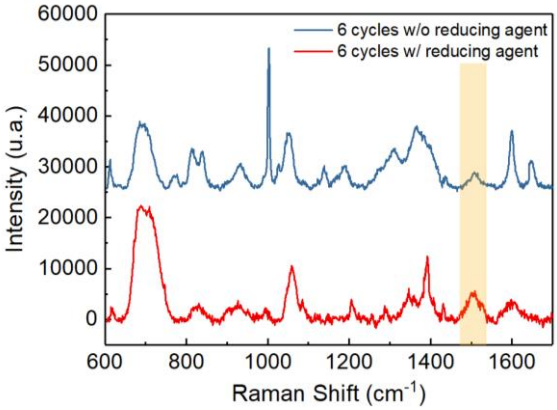

Figure 3.9 - Three average measurements of rhodamine SERS spectra of the SILAR-synthesised AgNPs on Office paper with reducing agent (red) and without reducing agent (blue)

Figure 3.9 shows the SERS activity spectra of the two substrates containing silver nanoparticles whose synthesis included with (red) and without (blue) $NaBH_4$ as a reducing agent. Analysing the peak located at 1508 cm^{-1}, it's noticeable that the substrate with AgNPs synthesized with $NaBH_4$ reducing agent shows a peak in the said band. Also the substrate with AgNPs fabricated without $NaBH_4$ as reducing agent shows a visible small peak at 1508 cm^{-1}, indicated that it has some effectiveness in the SERS effect. As expected, the characteristic peak of rhodamine corresponding to the substrate with AgNPs synthesized with $NaBH_4$, shows higher intensity compared to the peak given by the Raman spectrum relative to the substrate with AgNPs synthesized without $NaBH_4$, where the nanoparticles were supposedly synthesized by the salt present on paper.

It was then decided to continue exploring this new synthesis, never reported before, as a more environmentally friendly and cheaper synthesis (since one of the reagents was removed). For this, new cycles were tested and re-evaluated in relation to their SERS efficiency with 10^{-6} M R6G. New cycles were tested. From 1 to 9 cycles of silver nanoparticle SILAR-synthesis without $NaBH_4$ as reducing agent were performed and the results are shown in the following figure. The measurement conditions were kept the same.

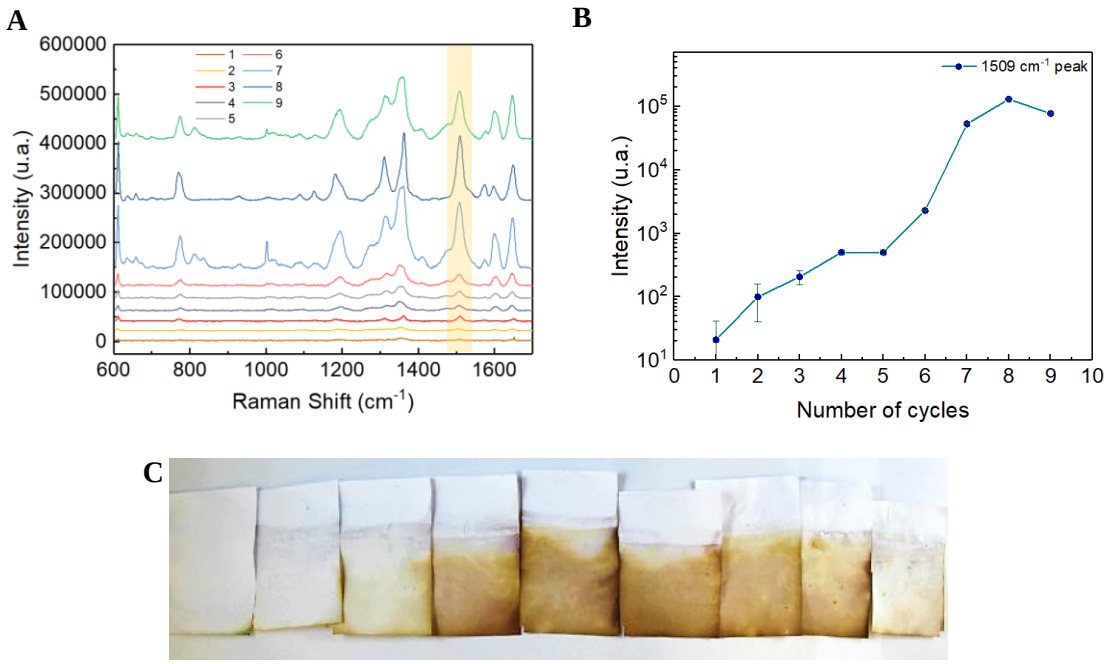

Figure 3.10 - A- 3 average measurements of rhodamine SERS spectra of the SILAR-synthesised AgNPs on Office paper from 1 to 9 cycles. B- intensities of 10^{-6} M R6G characterized peak at 1508 cm^{-1} with the number of SILAR cycles. The number of cycles and their intensities is plotted on the log scale because the intensity values of 1 to 6 cycles are very close to zero. C- Photo of the papers with the SILAR-synthesised AgNPs whitout reducing agent, from left to right: 1 to 9 cycles.

Obviously the first evidence that the reaction was actually occurring was the change in color from white (natural paper color) to brownish yellow **Figure 3.10-C**. This color change may be related to the size and shape of the nanoparticles formed in the paper fibers, because AgNPs have novel optical properties originated from coherent oscillation of the conduction electrons upon exposure to light impinges of specific wavelength, known as the localized surface plasmon resonance (LSPR), these optical characteristics depend on the size, shape and medium in which the NPs are inserted. AgNPs under 30 nm exhibit a yellowish color, and the zones of browner color that the papers present may be due to silver agglomerates[46].

The Raman peak intensity of R6G increases slightly from one to six SILAR cycles, then rises steeply up to seven cycles and continues to increase up to eight cycles where also shows a reduction of the substrate background noise, which ultimately drops significantly at nine cycles and the peak also broaden **(Figure 3.10-A, B**). It was then concluded that 8 is the best number of cycles to perform in this new synthesis.

To prove and visualize that nanoparticles were being formed, SEM and SEM-EDS analysis was done to the substrate whose number of SILAR-cycles showed better SERS efficiency (8 cycles), and the size of the nanoparticles was determined through imageJ software.

Through EDS analysis (**Figure 3.11-A**), the peak represented at E = 3 keV is related to silver, which confirms that AgNPs are being formed by this synthesis. It's possible to observe that small particles were formed on the paper fibers with the average NPs diameter size of 45.23±5.23 nm. The formed NPs have an oval shape and are present singularly or in small clusters.

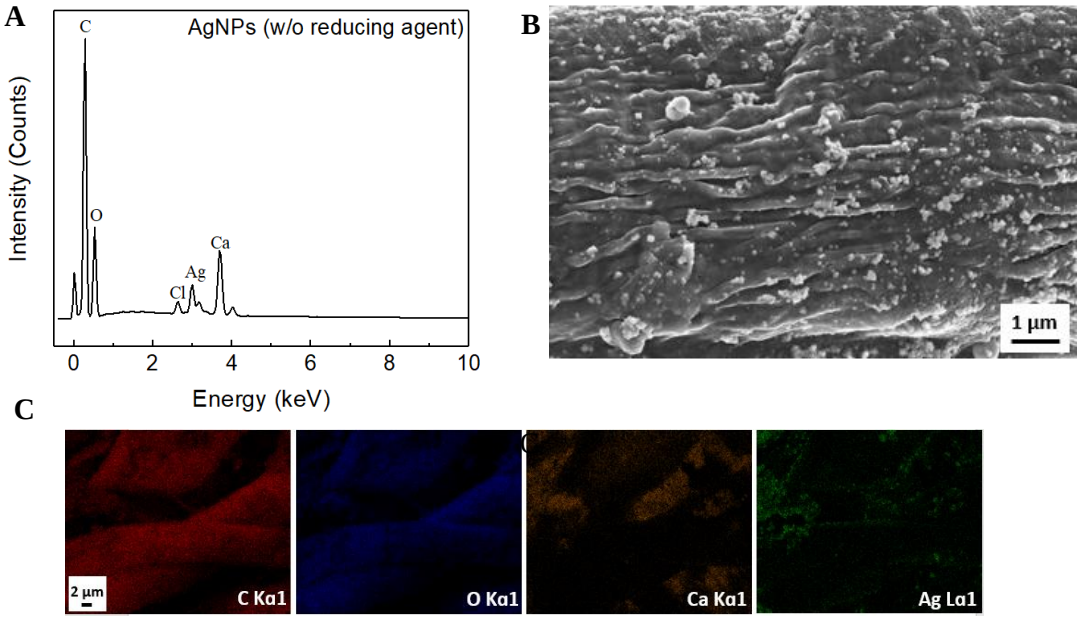

Figure 3.11 - A- EDS analysis of the substrate with AgNPs synthesized without $NaBH_4$ as reducing agent. B- SEM image of AgNPs 8 cycle SILAR-synthesised without $NaBH_4$ reducing agent. C- Distribution map of the substrates whose where AgNPs were SILAR-synthesised without $NaBH_4$ as reducing agent.

The distribution map of the office paper with AgNPs synthesized without $NaBH_4$ is also represented. The C and O represented in red and blue, respectively, covers the majority of the fibers since they are made of cellulose. The distribution map related to Ca (yellow) shows that the salt are located between fibers and comparing to the distribution map of silver (green), it's remarked that the Ag concentrates in the places there is more Ca, suggesting once again that in fact silver is reduced by $CaCO_3$.

Such as the optimum number of cycles to be performed, the optimum time that each step, corresponding to one cycle, must be investigated to in order to obtain the highest possible SERS effect. Times were tested from 10 to 50 sec, adding another 10 secs to the previous time, and the results are represented at **Figure 3.12**.

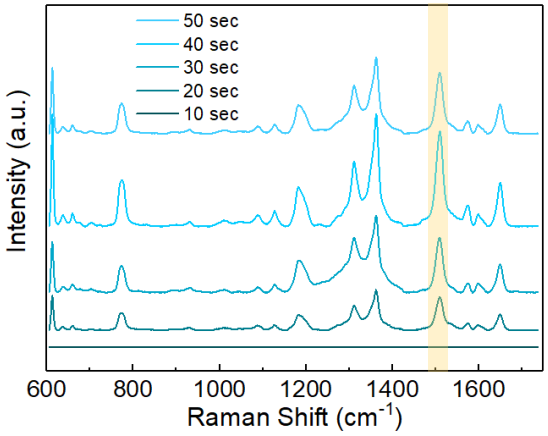

Figure 3.12 - Three average measurements of rhodamine SERS spectra of the SILAR-synthesised AgNPs on Office paper varying the time of each step cycle: 10, 20, 30, 40 and 50 secs.

To each substrate 3 random points were chosen and spectra were obtained, and the mean of the data is represented in the figure. Data were also normalized for comparison purposes.

The number of cycles (8 cycles) was maintained the same, but the time of each step of each cycle was varied. The tested times were 10, 20, 30, 40 and 50 secs. Between 10 and 30 secs (the latter used as the previous synthesis time) an increase in SERS activity is confirmed, as was already predicted and studied[28].

However, by increasing the synthesis time (i.e., time in which the paper is treated in each solution) from 30 to 40 secs, there is an even greater increase in SERS activity. By increasing more 10 secs, the intensity of the peak at 1508 cm^{-1} decreases again, possibly aggravated by the coalescence of the silver nanoparticles, since this is a SILAR-synthesis of layer by layer ionic adsorption and reaction, causing a decrease of "hot-spots" and consequently a decrease in SERS efficiency. Reaching the conclusion that 40 secs would be the ideal time to be used in the synthesis AgNPs through the two-stage SILAR technique without $NaBH_4$ as reducing agent.

Now that the AgNPs synthesis conditions are optimized: 8 SILAR cycles and duration of each cycle step of 40 sec. It's time to investigate the best conditions for the SILAR-synthesis of the gold nanoparticles that will decorate the Silver core in order to increase the SERS signal and also increase the shelf-life time of the substrate. It was also suspect that with this new synthesis of AgNPs without $NaBH_4$ as a reducing agent, gold plays an even more important role in the stability of silver nanoparticles. It was decided that the gold synthesis conditions would be maintained as: 1mM of $HAuCl_4$ and $NaBH_4$, and 30 secs of each synthesis step, since the goal wasn't to get the silver core completely decorated with gold NPs risking losing SERS efficiency, so that the signal obtained is not mostly of gold but of silver, since AuNPs led to a low Raman intensity compared to the AgNPs[28], just the enough to increase the shelf-life of the substrate. Therefore, several gold SILAR cycles were tested and the results are shown in **Figure 3.13**.

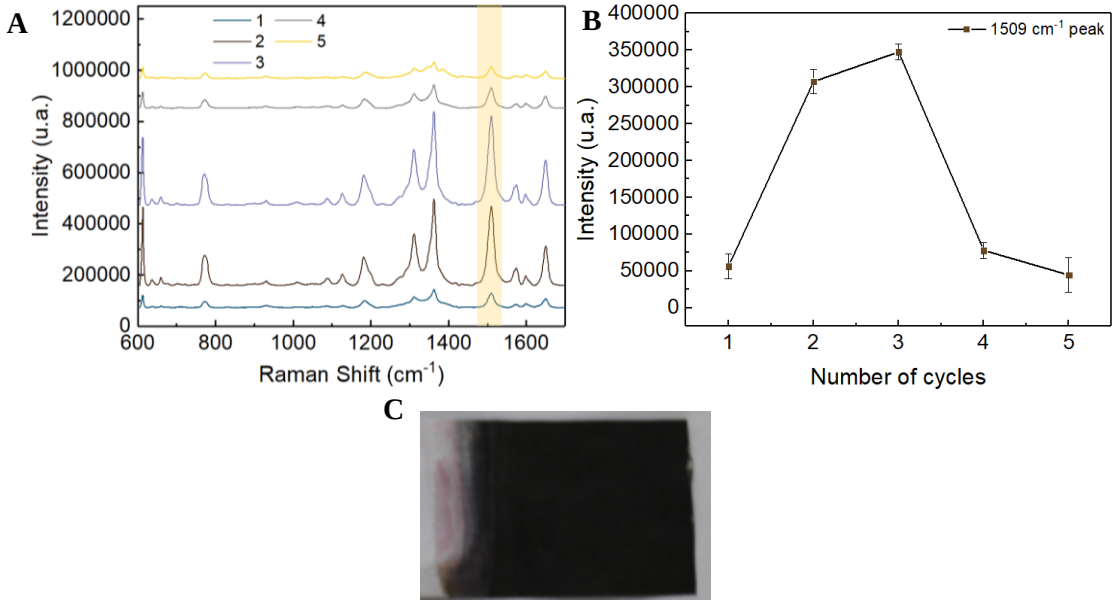

Figure 3.13 - A- Raman spectra and B- intensities of 10^{-6} M R6G characteristic peak at 1508 cm^{-1} with the number of SILAR cycles for decorating the shell AuNPs on the core AgNPs. C-photo of the substrate after the Ag@AuNPs were synthesized by SILAR method.

Also for these measurements, the conditions were kept the same. The used laser was maintained such as the exposure time and number of accumulations. The laser power was increased to 5% which demonstrated a less noise signal. For these measurements 10^{-6} M rhodamine was used as a reference and the characteristic peak at 1508 cm^{-1} was analysed. The Raman intensities greatly increase from 1 to 2 cycles and slightly increase up to 3 SILAR cycles and greatly decreased for 4 and 5 SILAR cycles perhaps due to the full coverage of the silver

nanoparticles core by gold nanoparticles and only the gold was the biggest contributor to the SERS signal.

Two and three SILAR cycles were chosen with relatively small variations in terms of Raman intensities, however 3 cycles presented higher Raman intensity and was selected as an optimal SILAR number of SILAR cycles for decorating the shell AuNPs on the core AgNPs. After the synthesis of the bimetallic NPs, the Office paper presented a very dark colour near the black, suggesting that possibly its surface is almost totally covered by nanoparticles. It's possible that at the end of the Ag synthesis cycles some $AgNO_3$ remains trapped in the paper fibers, which can be reduced by $NaBH_4$ used in the Au shell synthesis, thus increasing the amount of detected silver. Hydrophobic margins made with wax were also tested (small circles with 2 mm diameter were designed in the Adobe Illustrator software and printed with the XEROX ColorQube printer, in order to facilitate the SERS measurements, however with the paper colour it became impossible to distinguish the margins. Since the synthesis of the NPs is carried out directly on the paper consisting on dipping the paper itself into solutions, it was found that the NPs were also formed above the hydrophobic barriers and then that part was discarded.

Also the sensitivity of this new substrate was tested. Rhodamine was used at 7 different concentrations of 10^{-6} to 10^{-12} M, 3 spectra were collected at each concentration, normalized, and the mean of them is shown in **Figure 3.14**.

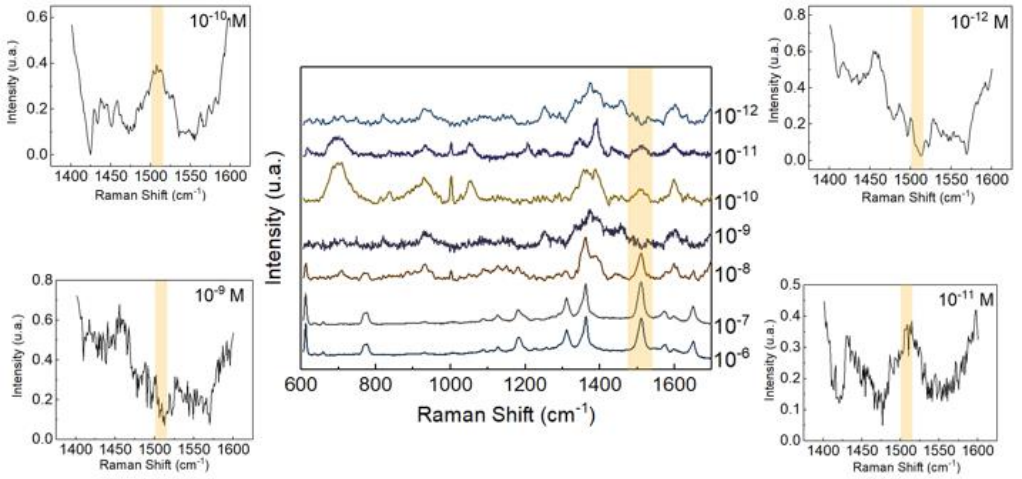

Figure 3.14 - Three measurement average of rhodamine SERS spectra on the optimized SILAR-synthesised Ag@AuNPs (AgNPs synthesis without $NaBH_4$ as reducing agent) on Office paper support with different concentrations. (Left) zoom of the 1508 cm^{-1} peak range for 10^{-9} M and 10^{-10} M. (Right) zoom of the 1508 cm^{-1} peak range for 10^{-11} M and 10^{-12} M.

The measurement conditions were kept the same, showing a cleaner signal and with more intense peaks (10 secs of exposure time, 5% of laser power, 10 accumulations), the laser used was 633 nm. Therefore, it's noted that from concentrations starting at 10^{-6} M to 10^{-8} M R6G the spectrum shows well-defined characteristic peaks. The same problem found in the other substrates is also notable in this one, it does not show any peak at 1508 cm^{-1} at concentrations of 10^{-9} M R6G, suggesting that the solution surely degraded (Left zoom). However, for concentrations relative to 10^{-10} and 10^{-11} M it's possible to perfectly distinguish the peak located at 1508 cm-1 although the peaks are broad and slightly overlapping with other peaks. For higher concentrations, the substrate does not exhibit any sensitivity. It is concluded that the limit of detection (LOD) is retained for concentrations of 10^{-11} M R6G. Important note: the laser power was decreased to 1% for measurements of R6G concentrations greater than 10^{-9} M. The EF was also calculated and the result was 3.5×10^5, the biggest result so far. The Office paper was the one that presented better

EF values comparing with Whatman nº1 paper, indicating that the office paper is in fact the best paper to be used in this type of synthesis.

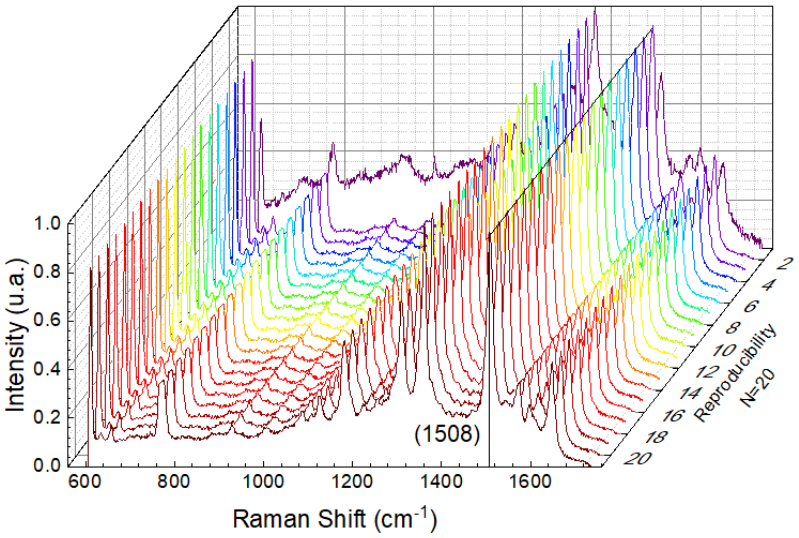

Figure 3.15 - Homogeneity tests of Office paper SERS substrate with Ag@AuNPs.

Homogeneity testes were done, and results are shown at **Figure 3.15**, this substrate comparing to others presents a really good consistency of spectra. The 20 measurements (made from different samples of the same substrate) show very good results. The characteristic peak of rhodamine under study is always of the same magnitude and well-defined.

The comparison spectra of the Ag@AuNPs SILAR-synthesised on Whatman and Office paper are shown at **Appendix C, Figure C3**. It's noticeable that the spectra given by the recent optimized SERS substrate presents more defined peaks, and it's also possible to see that the background effect is lower compared to the substrate with Ag@AuNPs, where the AgNPs were reduced with $NaBH_4$.

Stability tests were also done and presented on **Appendix C, Figure C4**.

This substrate was considered as the most optimized and was chosen for further characterization: XPS, XRD, SEM, SEM-EDS and biological tests.

3.2.3 SILAR-synthesized Ag@AuNPs on different papers: comparison

The bimetallic Ag@AuNPs synthesized directly on the different papers (whatman nº1 and office Paper) were characterized through various assessments. Essentially the characterization was done between whatman paper whose NPs were synthesized through the previously optimized SILAR-synthesis, and the office paper whose NPs were synthesized by the recent optimized SILAR-synthesis in which the AgNPs were synthesized without $NaBH_4$ as reducing agent

An XPS analysis based on high detection limit and precision, was performed to confirm not only the existence of gold and silver in the substrates, but also the coordination of these two noble metals on the surface of the cellulose fibres. The obtained spectra are represented in

Figure 3.16.

In both papers (Whatman and Office) (

Figure 3.16-**A, B**), the peaks centred at 285.9 eV and 531.9 eV, associated with carbon (C1s) and oxygen (O1s) respectively, confirms the signature of the cellulose structure (the main component of paper fibres) $(C_6H_{10}O_5)_n$ [28].

Also in both papers, the bands fixed at 85 and 370 eV confirm the coordination of the monometallic structures, gold (Au 4f) and silver (Ag 3d) respectively, with the cellulose group[47].

Figure 3.16-**A1, B1** shows the detailed spectra of Au4f and Ag3d regions, on whatman nº1 and on office paper, respectively. The two new peaks at 83.9 and 86.9 eV on whatman paper,

Figure 3.16-**A1** and the two new peaks centred at 83.8 and 87.3 eV on office paper

Figure 3.16-B1 are related to $Au4f_{7/2}$ and $Au4f_{5/2}$. Also, the two new peaks at 368 and 373.9 eV on Whatman nº1 paper and the two peaks located at 367.8 and 373.8 eV referring to Office are related to $Ag3d_{5/2}$ and $Ag3d_{3/2}$, respectively. The differences between the $4f_{7/2}$ and $4f_{5/2}$ peaks for gold (3 eV and 3.5 eV) as well as between the $3d_{5/2}$ and $3d_{3/2}$ peaks for silver (5.9 eV and 6 eV) on whatman and office paper, respectively, were also the same as the handbook values of zero valence gold and silver[48,47]. This observation suggests that the majority of the gold and silver atoms should exist in zero valence state (Au^0 and Ag^0) as well as highly crystalline particles in spite of ionic reaction of SILAR technique[28-47]. XPS findings confirmed the grafting of cellulose, AgNPs, and AuNPs.

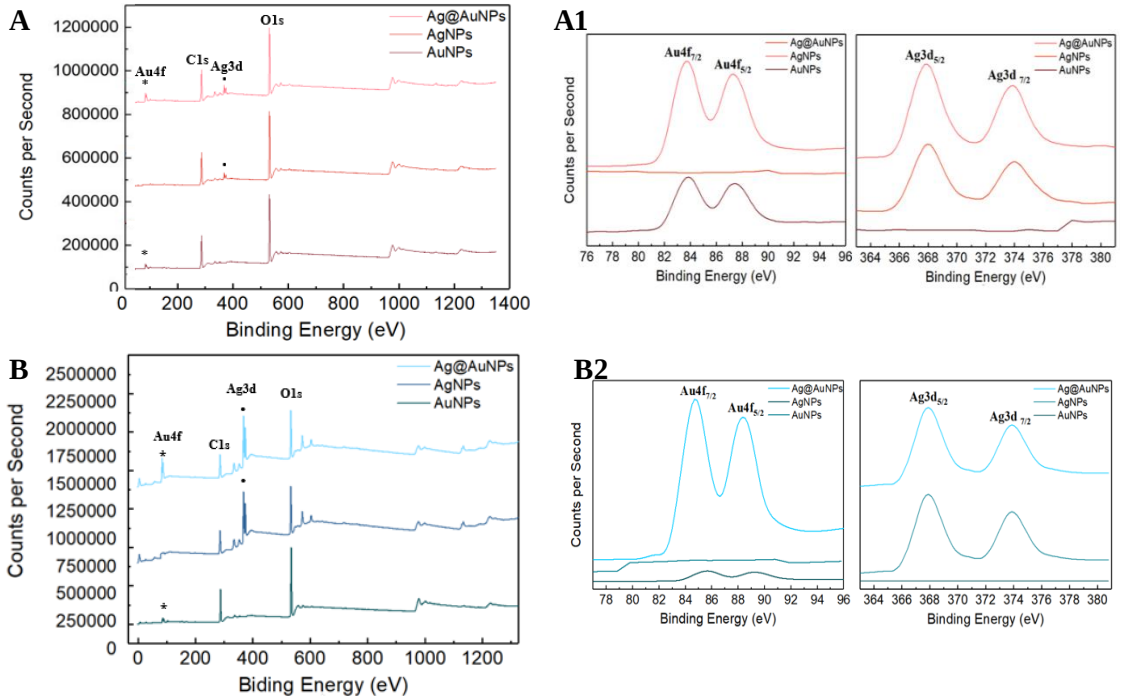

Figure 3.16 - (A) XPS spectra of the previously optimized SILAR-synthesised AuNPs, AgNPs and Ag@AuNPs on Whatman paper; (B) XPS spectra of the recent optimized SILAR-synthesised AuNPs, AgNPs and Ag@AuNPs on office paper. (A1) and (B1) Zoomed part of the spectrum relative to gold and silver peaks.

Also, by calculating the silver and gold Auger parameter and comparing to the literature, it is possible to conclude that the Ag and Au signal is in fact from metallic structures, therefore proving nanoparticle formation since this parameter is particularly useful for chemical state analysis and can be used without interference of surface charging (presented and further discussed in **Appendix D, D1**).

However, another fact stand out: the intensity of the peaks corresponding to silver and gold in the office paper are far higher than that observed in Whatman, confirming the suspicion that there would be a higher concentration of these metals on the surface, since this is a method of quantitative surface analysis[49], that may be due, once again, the high hydrophobicity and low porosity of this paper. But also raised the suspicion that the $CaCO_3$ present in the paper itself was helping during the formation of NPs. The elements quantification is presented in **Table 3.2.**

Table 3.2 - XPS element quantification for the different papers.

Type of paper	Element Mass %					
	O	C	Ag	Au	Cl	N
Whatman nº1	38.46±0.2	58.11±0.2	1.43±0.21	1.00±0.2	-	1.04±0.18
Office	33.30±0.2	60.70±0.21	3.6±0.2	2.1±0.22	0.2±0.1	-

As expected, the amount of mass% of the metallic elements (silver and gold) is higher in office paper than in Whatman paper. In office paper, due to its low porosity, it was expected that these elements would be retained at the surface. Elements like Chlorine (Cl) should be related to the mineral Calcite ($CaCO_3$) present only on office paper and the Nitrogen (N) must be related to the $AgNO_3$ residues used in the synthesis of silver. All quantifications and assessments were made through ESCAPE software.

XPS analysis was also done on the SERS substrates with Ag@AuNPs bimetallic nanoparticles synthesized without $NaBH_4$ as silver reducing agent (**Figure 3.17-A**), in which one of the substrates the time of each cycle step was 30 secs and in the other was 40 secs.

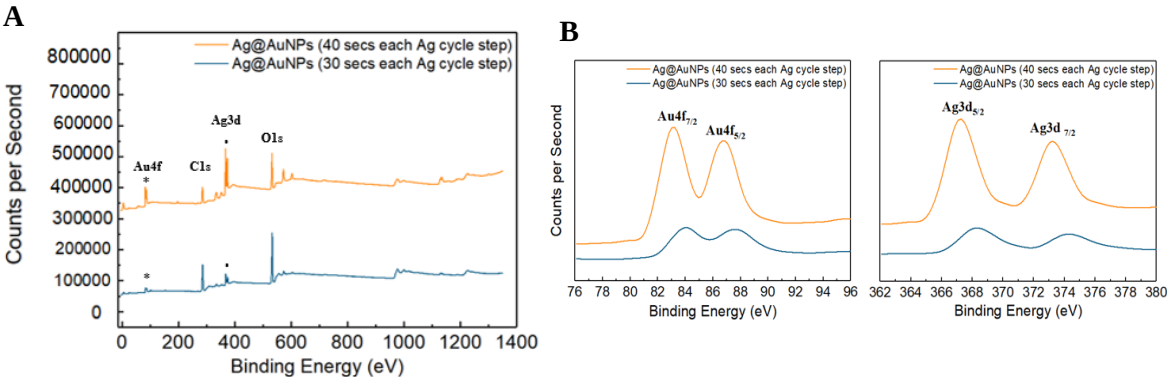

Figure 3.17 - (A) XPS spectra of the SILAR-synthesised Ag@AuNPs on Office paper without $NaBH_4$ as reducing agent of silver synthesis with differences in synthesis time: 30 (blue) and 40 secs (orange) each cycle step; (B) Zoomed part of the spectrum relative to gold (Au4f) and silver (Ag3d) peaks.

On **Figure 3.17– (B)** shows the detailed spectra of Au 4f and Ag 3d regions, of both substrates. The two peaks located at 83.4 and 86.7 eV are related to Au4f7/2 and Au4f5/2. Also the two new peaks located at 367.2 and 373.2 eV are related to Ag3d5/2 and Ag3d3/2, respectively. This observation suggests that the majority of the gold and silver atoms should exist in zero valence state (Au^0 and Ag^0) as well as highly crystalline particles in spite of ionic reaction of SILAR technique[28,47]. XPS findings also confirmed the grafting of cellulose, AgNPs, and AuNPs.

It's clear that the peaks related to Au4f and Ag3d regions of the spectrum representing the substrate whose each step of Ag SILAR-synthesis cycle was 40 secs (orange), have a much higher intensity compared to the other (blue), indicating that, on the surface, the concentration of metals is superior.

Furthermore, it was used XRD analysis in order to confirm the chemical composition of the nanostructures deposited in the two different papers **(Figure 3.18)**.

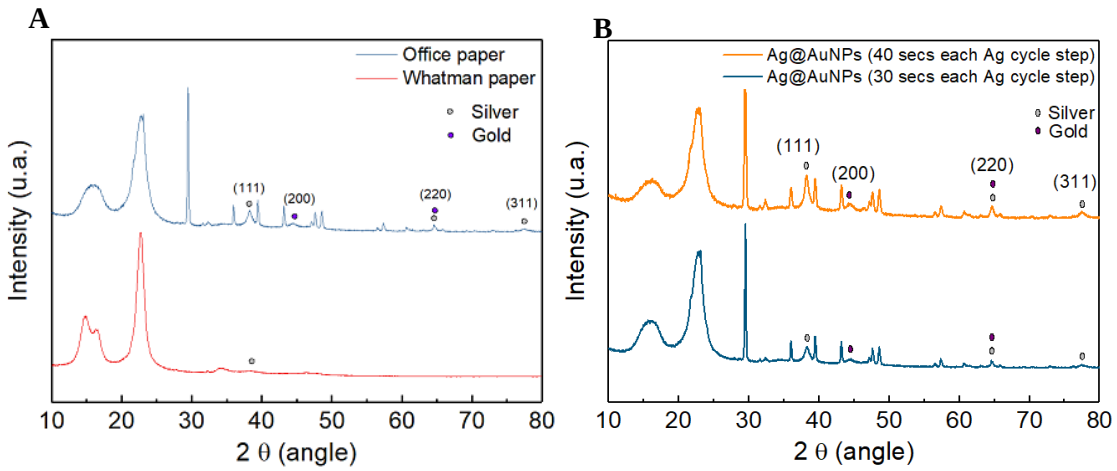

Figure 3.18 A- XRD diffractograms of office paper (blue) and Whatman paper (red) with SILAR-synthesised bimetallic nanoparticles Ag@AuNPs. B- XRD diffractograms of Ag@AuNPs SILAR-synthesised on Office paper without $NaBH_4$ as reducing agent of silver NPs with differences in synthesis time: 30 (blue) and 40 secs(orange) each cycle step.

Besides to the cellulose peaks found in both papers substrates and the calcite peaks present in the office paper, when comparing whatman and office paper (**Figure 3.18- A**) the prominent peaks of AgNPs, almost exclusively found on office paper, were observed at 38.1º, 64.5º and 77.5º in 2θ values, indexed as (111), (220) and (311) diffractions, respectively[50], this reflection planes correspond to the face-centred cubic (fcc) structure of Ag and Au planes. While that, the gold peak was found exclusively on the office paper at 44.3º and 64.7º in 2θ values indexed as (200) and (220). The 2θ values of silver and gold crystals are very close to each other (**Appendix D**, **table D2**), due to their very similar lattice constants (JCPDS No. 04-0783) and thus the peaks of gold and silver corresponding to (220) diffractions overlapped. Only a small amount of silver was detected in the Whatman paper, indicating that the nanoparticles formed by this type of synthesis must penetrate deeper into Whatman paper than the Office paper where they prevail on the surface (important feature for SERS). Also, the small peaks of gold are related to the reduced amount used in the synthesis (1 mM of $HAuCl_4$). This finding is consistent with the presence of weak gold peaks for bimetallic Ag@AuNPs and AuNPs in XPS analysis.

Figure 3.18-B shows the XRD patterns of office paper with Ag@AuNPs synthesized by the recent optimized SILAR-synthesis, whose Ag synthesis was synthesized with 30 secs (blue) and with 40 secs (orange) each step of SILAR-cycle. It's notable that the substrate, in which the synthesis took longer, presents peaks referring to Ag and Au of greater intensity and more well-defined, indicating, that more silver is actually being formed with increasing the synthesis time.

SEM-EDS complementary analysis was carried out on whatman and office paper substrates (**Figure 3.19**). Besides the carbon and oxygen peaks related to the cellulose, the peak of gold (E = 2.12 keV) and the peak of silver at (E = 3 keV) also stand out. It is clearly visible that in whatman paper these peaks are barely evident compared to office paper, whose SILAR-synthesis was recently optimized. In the **Appendix D3** are shown the tables of EDS results where it's possible to see that this substrate actually exhibits greater relative amount of silver in weight% and atomic concentration. The peak corresponding to Ca (E = 3.68 keV), only visible in the office paper, related to the $CaCO_3$ present only in this, it is hardly evident, indicating that the salt is actually being consumed and used for the reduction of AgNPs.

The distribution map of the detected elements represented in the spectra was made and is represented in **Figure 3.19-C**. As was already suggested in the spectrum, Ca basically ceased to

exist (represented in orange). The silver (green) has an intense color and is concentrated between fibers, where remains of Ca can still be seen. The distribution maps shows that gold (yellow) and silver are concentrated in the same areas, with silver having a more intense color than gold, suggesting that, in fact, silver nanoparticles are not completely covered by gold, hoping this gold quantity will be enough to increase the shelf-life of the SERS substrate.

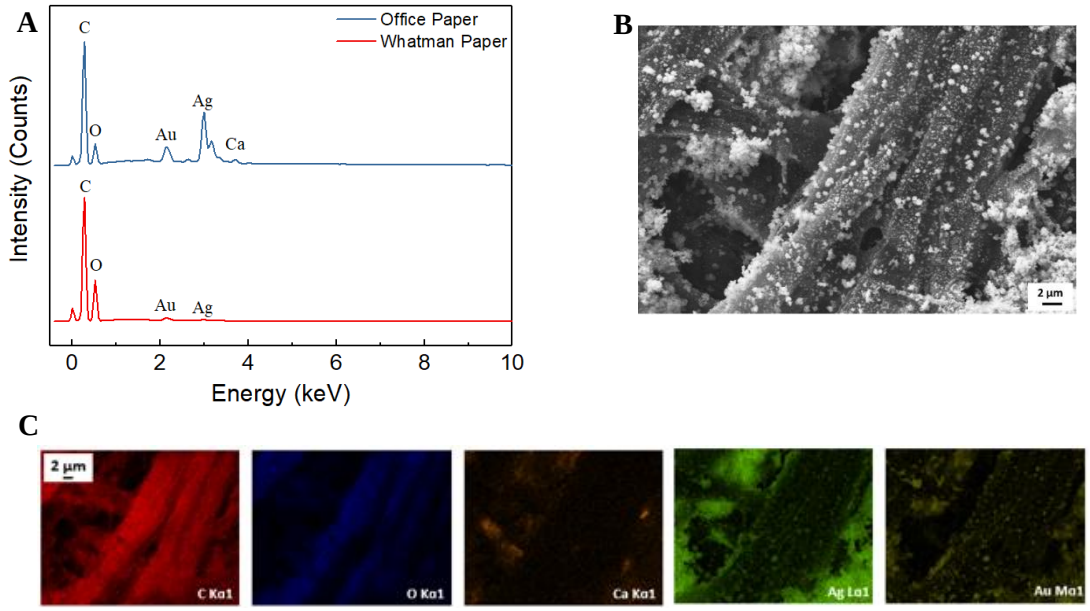

Figure 3.19 - EDS analysis of the Whatman com Ag@AuNPs synthesized with the previously optimized SILAR-synthesis (red) and the Office paper with Ag@AuNPs synthesised with the recent optimized SILAR-synthesis (blue). C- EDS image and B- Distribution maps of the office substrate.

SEM images were also obtained (**Figure 3.20**) in order to observe the presence of the nanoparticles in the paper's fibres to have a morphological characterization of the substrate. The magnifications used was 5 kx and 10 kx. It wasn't possible to use higher acceleration voltages, since the destruction of the cellulose fibres was observed. It's confirmed that in both papers, the formed nanoparticles led to a raspberry-like structure composed of a core AgNP decorated with a lot of AuNPs. Since the SILAR technique is the layer-by-layer deposition, a gold component on the silver surface is coated in the form of thin layer or nanoparticles. Most studies have been made an effort to synthesize a complete core@shell nanoparticle structure[28,51,52]. However, it wasn't consider a bimetallic nanostructure that the core was completely covered up with the shell, because a compact shell layer or increasing of AuNPs resulted in the decreasing of SERS efficiency (**Appendix C1**). It's visible that the nanoparticles formed in both papers have a raspberry shape, although it's not possible to determine with SEM that the nanoparticles are actually formed by the Ag core. However with TEM analysis it would be possible to have this confirmation, although it was not possible to do it, it was already done by *Wansun Kim et al*[28], with the particularity that the Ag@AuNPs would have to be synthesized directly on the grid by the two stage SILAR-synthesis, since the paper substrates does not transmit through electron, the paper-deposited nanoparticles could not be directly measured by high accelerating electrons such as TEM or focused ion beam (FIB). Their experiments showed that by this technique tiny AuNPs were attached to AgNPs core, forming bimetallic nanostructures with a raspberry shape where gold NPs are closely packed with only a few nanometers of separation.

Comparing the two papers, it's observed that in whatman paper, the formed NPs are more distant and, in less quantity, than in office paper, as was already suggested by the EDS spectrum. In office paper, virtually all the fibers are evenly covered by the formed NPs of various sizes with

small NPs and big clusters. Due to the low porosity of the paper, their ability to retain NPs on the surface is greater, leaving no space for them to penetrate into the paper. Which translates into an important feature on SERS substrates, increasing the rugosity of the substrate for the creation of "hot-spots" (an indispensable characteristic in SERS single molecule detection).
The mean values of the nanoparticles are shown in **Table 3.3**.

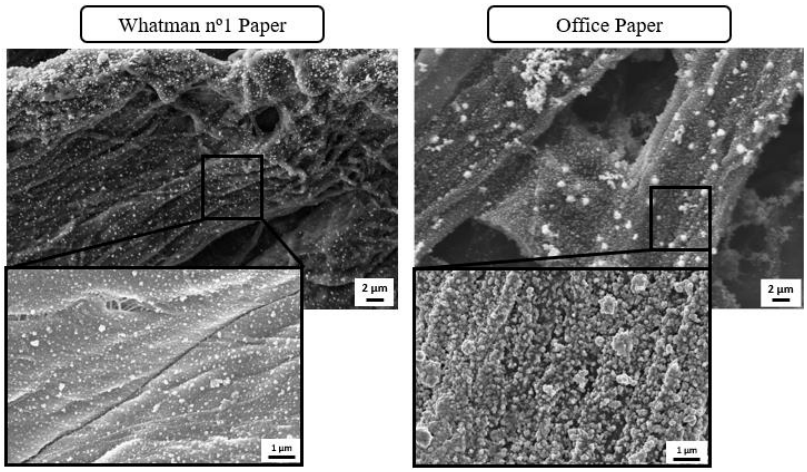

Figure 3.20 - SEM images of the Ag@AuNPs synthesized by the two-stage SILAR technique on Whatman nº1 paper and Office paper.

The values represented in **Table 3.3** were obtained through the ImageJ software. Values were based on the nanoparticle shape, where for each analysed nanoparticle several diameters were measured, and their mean value was calculated and used for the final NPs sizes and standard deviations calculations.

Table 3.3 - Mean values of bimetallic nanoparticle diameters on Whatman and Office paper

Nanoparticle structure	Particle Size (nm)	
	Whatman nº1	Office
Clusters	223.34±54.32	85.33±22.40
Small nanoparticles	97.01±20.76	38.81±16.15

After characterizing both substrates containing bimetallic nanoparticles, office paper was chosen as the best and most optimized, due to its high EF, higher amount of Ag and Au and greater capability to retain NPs to the surface, demonstrating a higher sensitivity in SERS signal and for its greener and environmentally friendly synthesis. The office paper containing Ag@AuNPs whose AgNPs synthesis was performed without $NaBH_4$ as the reducing agent and with 40 secs each Ag cycle step was chosen for the following biological tests.

3.2.4 Optimized SILAR-synthesized Ag@AuNPs on Office paper: Biological tests

The biological tests were carried out on the recently optimized substrate (Office paper with bimetallic nanoparticles). Firstly, the tests consisted on measuring the control solution (PBS), tumoral (MDA-MB-231) and non-tumoral exosomes (MCF-10A) in order to see if it was possible to distinguish between spectra of both samples (**Figure 3.21-B**). Concluding whether the substrate is effective in detecting exosomes. The exosomes sample used in all measurements had concentration of 10^9 particles/mL. For all biological tests, it was concluded that the best laser to

be used was 532 nm, since no fluorescence problems were verified and showed an improvement in substrate sensitivity.

To test the capability of differentiation between the SERS spectra, corresponding to PBS, tumoral and non-tumoral exosomes, the Principal Component Analysis (PCA) was performed. PCA was applied since this a statistical analysis tool utilized to investigate the major patterns in datasets, where a smaller number of uncorrelated variables, called "principal components", are identified by analysing variances in each collected spectrum and grouping the similar ones, until association between different groups is possible through 95% confidence ellipses surrounding that groups. When the patterns are identified in the set, the number of analysed dimensions can be reduced without a significant loss of information, and a thousands of Raman spectra can be plotted into a XY axis scatter graphic. The two principal components used to the score plot were the Principal Component 1 (PC1) and the Principal Component 2 (PC2).

Although the exosomes used in this work are from the same cell line, the obtained Raman spectra present different fingerprints. Since they are constituted by different proteins, even when they have the same origin. Also, the way they lie on the substrate and which part of the exosome is hit by the laser will influence the obtained spectra, however, exosomes from the same stem cells demonstrate common patterns in the spectra obtained, these common patterns will be further analysed by PCA.

To each acquire spectrum was subtracted the baseline and normalized the data using the WiRE™ software. The smooth tool was not applied because it was possible the loss of spectrum information. The **Figure 3.21-B** shows the mean Raman spectra of PBS and the exosomes, each of which 35 spectra was collected.

By analysing the mean spectra referring to PBS , MCF-10A (non-tumoral) and MDA-MB-231 (tumoral) exosomes (**Figure 3.21-B**) it's possible to observe that there are significant differences between them (peaks with most variance between groups are highlighted in pink**)** and by the score plot given by the PCA analysis was confirm that there is a clear distinction between the samples, since the 95% confidence ellipses do not overlap.

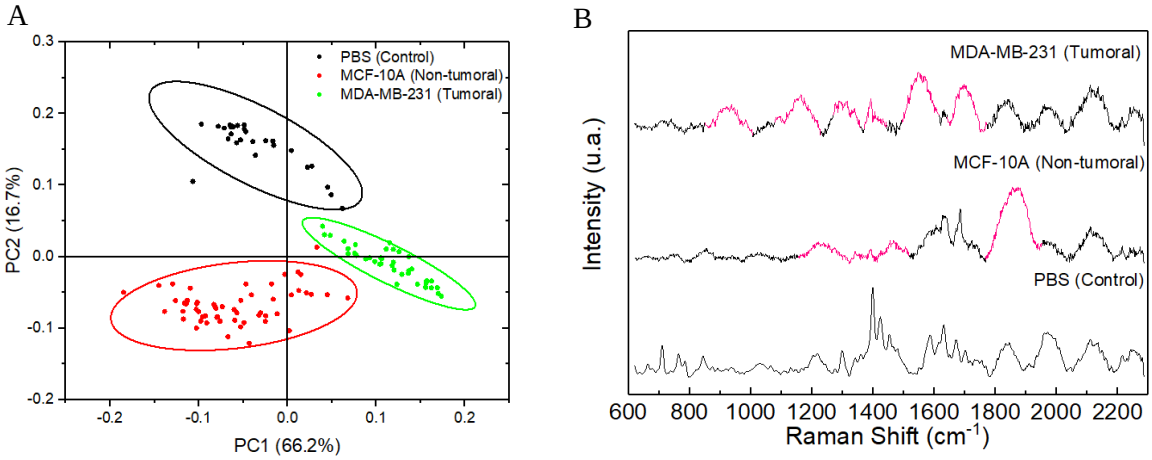

Figure 3.21 - PCA resultant score plot using PC1 and PC2 as the analysed principal components: PBS (control) in black, MCF-10A (red) and MDA-MB-231 (green) exosome sample analysed. (B) Average PBS, MCF-10A and MDA-MB-231 Raman spectrum: spectra peaks with most variance between groups highlighted in pink.

Visualizing the loading plot, present in **Appendix E, Figure E1**, it is possible to see which wavenumbers contribute with the most variance to PC1, in this case all the wavenumber of the spectra equally contributed positively to the variance PC1 analysis. The success of this test is due

to the low contribution of cellulose, present in the substrate, which could overlap with the contribution of biological samples, since they are constituted by proteins, lipids, DNA among others, which in turn are composed of C, O e H bonds, corresponding to the cellulose nature.

It's also possible to use the PCA method as a real-time diagnostic method, ie, using the 95% confidence ellipses, if a spectrum to be analysed is located inside these ellipses it's safe to assure with 95% confidence that this spectrum belongs to the group that is inserted. These tests were performed and are present in the **Appendix E2**.

A cost analysis was also performed based on reagent prices on Sigma-Aldrich® and papers used. For the previously optimized SILAR synthesis in which $NaBH_4$ is used as reducing agent of AgNPs in Whatman nº1 paper the cost of production is 2.24 € and in the Office paper it's 1.97 €. For the new SILAR-synthesis in which $NABH_4$ is not used as reducing agent of AgNPs, a production cost of 1.93 € was estimated for the office paper. The synthesis made in the Office paper have a lower cost because this paper is a common material compared to Whatman nº1 paper, also the new synthesis presents a lower monetary value because $NaBH_4$ of 20 mM concentration is not used in the formation cycle of the silver nanoparticles.

4 Conclusion and futures perspectives

This work has as main objective the development of effective SERS substrates in the detection and distinction of biological samples of non-tumoral and tumoral exosomes from breast cancer cells. The paper-based SERS substrate is a disposable approach and two types of paper were investigated: Whatman no.1 paper and Office paper. The use of paper as support for SERS substrates is an abundant, usable, cost-efficient and biodegradable alternative.

In both papers an *in situ* synthesis of bimetallic nanoparticles was carried out. Bimetallic nanoparticles consisting of a synthesis of Ag core nanoparticles (AgNP) and a synthesis of Au shell nanoparticles (AuNPs) were fabricated by the two-stage successive ionic layer absorption and reaction (SILAR) technique. Throughout the work, different conditions of synthesis were investigated and tests with R6G, as a label due its large effective cross-section that results in a strong SERS signal, were carried out in order to reach the most optimized SERS substrate. One of the concerns in the synthesis of bimetallic nanoparticles of silver and gold was to fabricate nanoparticles whose silver core was not completely covered by the gold shell, since silver shows a superior SERS signal compared to gold. However, the shelf-life of AgNPs-based substrates is inferior than those containing AuNPs, thus the gold is used with the aim of increasing the period in which the substrate remains active without losing much SERS efficiency.

The paper SERS substrates were analysed through XPS, XRD, SEM, SEM- EDS and Raman techniques.

The concentration of silver salt was always maintained the same in all experiments (20 mM). The first SILAR-synthesized assay, 6 SILAR cycles were performed in order to form the Ag-core of the bimetallic nanoparticles. Then two concentrations of gold salt were tested (1 and 10 mM). First, the highest concentration of gold was tested, whose SERS signal increased with the increase of the number of SILAR-cycles performed. However, compared with monometallic nanoparticles, it was concluded that gold mainly contributed to SERS effect. Then, the lower concentration was tested in order to reduce the gold contribution, concluding that 2 is the ideal number of SILAR-cycles for the formation of the Au-shell in Ag-core. This synthesis was performed in both papers and the SERS substrates were assayed for SERS efficiency.

Compared to Whatman nº1, Office paper has less porosity, which increases its surface and compact area, a characteristic that provides a higher concentration of NPs at the surface, since they have less space to penetrate deeper the paper. The porosity of the substrates proved to be one of the most important features in the development of SERS substrate. Another main characteristic of the Office paper was the presence of $CaCO_3$ impregnated between the fibers of the paper due to the treatment carried out in order to increase its whiteness. Another type of synthesis was investigated. In the SILAR-synthesis of AgNPs, the $NaBH_4$ step was removed and the reducing power of the salt present on the paper was investigated in order to make the substrate manufacturing process more environmentally friendly as well as cheaper. In addition to the number of cycles, also the time of SILAR-synthesis were tested, concluding that 8 cycles was the most indicated number of SILAR-cycles for the AgNPs formation and the time of each cycle step of 40 secs, showing the best SERS signal. By further increasing the step time, the SERS effect decreased, perhaps due to the coalescence of the NPS since this is an ionic adsorption and reaction technique also used in the production of films. By increasing the number of cycles, the size of the NPs will also increase and eventually coalescing forming a film. Characterization by XPS has shown that 0 valence metal (Ag^0) have indeed been created, and the SEM-EDS distribution maps indicate that silver nanoparticles are formed at sites where the $CaCO_3$ concentration is higher. The Au-shell was synthesized according to the previously tested conditions, with concentration of 1/1

mM $HAuCl_4$/$NaBH_4$ and 3 as the ideal number of SILAR-cycles to ensure that AgNPs are not fully covered by AuNPs. The optimized two-stage SILAR fabrication procedures led to the bimetallic nanoparticles (Ag@AuNPs) that showed a remarkable SERS effect when compared to monometallic ones AgNPs and AuNPs that did not demonstrate significant SERS effect when synthesized by this synthesis, however proved to increase the SERS signal when in the form of bimetallic nanoparticles along with the increased of shelf-life of the SERS substrates.

Utilization of the obtained composites as SERS substrates showed good results and fulfilling the objective of a low-cost substrate able to enhance Raman signal. All substrates demonstrated a shelf life of more than 1 month, demonstrating the role of gold was successful in delaying the early oxidation of silver. Both the Whatman nº1 and the Office paper showed equal LOD (10^{-11} M with R6G probe) in both synthesis, however the tests performed on Whatman paper demonstrated a more pronounced background noise as well as autofluorescence problems. Substrate synthesized with $NaBH_4$ as AgNPs reducing agent have a lower EF (10^4) comparing to the substrate synthesized with $CaCO_3$ as a reducing agent of AgNPs (10^5). The latter was evidentially better in discriminating peaks, reducing background noise and being overall more versatile on the detectable analyte, since there was almost no cellulose peaks interfering with the detection, all substrates demonstrated a better Raman signal when the analyte was measured as a drop than allowed to dry. The SILAR-synthesis may be applied to other types of support matrixes, as long as they carry the bimetallic nanoparticles as tetra pack and other cellulose papers or nanocellulose substrates can be studied. Also on a substrate of nanocellulose extracted from *Nata de Coco* was performed the previously optimized SILAR-synthesis, which proved to be an efficient SERS substrate, however degraded in a short time (less than one month), visually the substrate colour changed from orange to greyish, suggesting the aggregation of the nanoparticles, perhaps due to their poor adhesion to the nanofibers.

Tests with exosomes using PCA as a targeting and diagnostic method were not satisfactory for the substrates synthesized by the first synthesis, indicating that a high contribution of cellulose was overcoming the peaks given by the analyte. However, the substrate fabricated by the latest SILAR-synthesis showed almost no contribution of cellulose and good PCA results were achieved. Was possible to group data from control, tumoral and non-tumoral exosomes. Due to the fact that this substrate has shown good results, only proves that the contribution of cellulose is a disadvantage in this type of analysis when a very high sensitivity is necessary.

Other tests could be performed, other types of cancer could be tested, such as exosomes from different cell lines so as to possibly prove that the successful distinction of the data by PCA is not exclusive to this type of exosomes used, but may be applied to any other type of samples, in order to test this technique specificity using this SERS substrate.

Concluding, with this work, it was possible to optimize and fabricate a paper-based SERS substrate, with a very low price and an environmental friendly synthesis, using a regular office paper, that allow to distinguish non-tumoral from tumoral exosomes from breast cell lines, with a group confidence of 95%.

References

1. Key, T. J., Verkasalo, P. K. & Banks, E. Reviews Epidemiology of breast cancer. **44,** 133–140 (1865).
2. Asia, S., Asia, S. & Hdi, H. Source: Globocan 2018. **876,** 2018–2019 (2019).
3. Al-Hajj, M., Wicha, M. S., Benito-Hernandez, A., Morrison, S. J. & Clarke, M. F. Prospective identification of tumorigenic breast cancer cells. *Proc. Natl. Acad. Sci.* **100,** 3983–3988 (2003).
4. Biópsias. 1 (2017). at <https://www.saudecuf.pt/areas-clinicas/exames/ginecologia-obstetricia/biopsias>
5. Nounou, M. I. *et al.* Breast Cancer: Conventional Diagnosis and Treatment Modalities and Recent Patents and Technologies. *Breast Cancer (Auckl).* **9,** 17–34 (2015).
6. Wu, C.-Y., Du, S.-L., Zhang, J., Liang, A.-L. & Liu, Y.-J. Exosomes and breast cancer: a comprehensive review of novel therapeutic strategies from diagnosis to treatment. *Cancer Gene Ther.* **24,** 6–12 (2017).
7. Wei, Y., Lai, X., Yu, S. & Chen, S. Exosomal miR-221 / 222 enhances tamoxifen resistance in recipient ER-positive breast cancer cells. *Springer* 1–9 (2014). doi:10.1007/s10549-014-3037-0
8. Park, J. *et al.* Exosome Classification by Pattern Analysis of Surfaceenhanced Raman Spectroscopy Data for Lung Cancer Diagnosis. (2017). at <http://pubs.acs.org>
9. Harris, D. A., Patel, S. H., Gucek, M., Hendrix, A. & Westbroek, W. Exosomes Released from Breast Cancer Carcinomas Stimulate Cell Movement. *PLoS One* 1–18 (2015). doi:10.1371/journal.pone.0117495
10. Lee, C. *et al.* 3D plasmonic nanobowl platform for the study of exosomes in solution. *Nanoscale* **7,** 9290–9297 (2015).
11. Wang, J.-P. *et al.* The role of exosomal non-coding RNAs in cancer metastasis. *Oncotarget* **9,** 12487–12502 (2018).
12. Sivashanmugan, K. *et al.* Bimetallic nanoplasmonic gap-mode SERS substrate for lung normal and cancer-derived exosomes detection. *J. Taiwan Inst. Chem. Eng.* **80,** 149–155 (2017).
13. Al Ahmad, M. Electrical Detection, Identification, and Quantification of Exosomes. *IEEE Access* **6,** 22817–22826 (2018).
14. Mahmood, T. & Yang, P. C. Western blot: Technique, theory, and trouble shooting. *N. Am. J. Med. Sci.* **4,** 429–434 (2012).
15. Gholizadeh, S. *et al.* Microfluidic approaches for isolation, detection, and characterization of extracellular vesicles: Current status and future directions. *Biosens. Bioelectron.* **91,** 588–605 (2017).
16. Feng, S. *et al.* Biosensors and Bioelectronics Nasopharyngeal cancer detection based on blood plasma surface-enhanced Raman spectroscopy and multivariate analysis. *Biosens. Bioelectron.* **25,** 2414–2419 (2010).
17. Sharma, S. K. Biomedical Applications of Micro-Raman and Surface-Enhanced Raman Scattering (SERS) Technology. **8025 80250,** 1–70 (2012).

18. Stremersch, S. *et al*. Identification of Individual Exosome-Like Vesicles by Surface Enhanced Raman Spectroscopy. *Small* **12,** 3292–3301 (2016).
19. Huang, N. *et al*. Full range characterization of the Raman spectra of organs in a murine model. *Opt. Express* **19,** 22892 (2011).
20. Mulvaney, S. P. & Keating, C. D. Raman Spectroscopy. *Anal. Chem.* **72,** 145–158 (2000).
21. Jo, M. & Oliveira, Q. De. Plasmonic substrates for ultrasensitive surface- enhanced Raman spectroscopy : application to the detection of food toxins. (Faculdade de Ciências e Tecnologia e a Universidade Nova de Lisboa, 2015).
22. Stiles, P. L., Dieringer, J. A., Shah, N. C. & Van Duyne, R. P. Surface-Enhanced Raman Spectroscopy. *Annu. Rev. Anal. Chem.* **1,** 601–626 (2008).
23. Howes, P. D., Rana, S. & Stevens, M. M. Plasmonic nanomaterials for biodiagnostics. *R. Soc. Chem.* 1–19 (2014). doi:10.1039/c3cs60346f
24. Kneipp, K. Martin Moskovits , Department of Chemical Engineering , The City College of the City University of New York , New York , NY 10024 , USA. 195–203 (2012).
25. Sur, U. K. Surface-Enhanced Raman Scattering. *Raman Spectrosc. Appl.* **27,** 241–250 (2017).
26. Tan, C. L., Lee, S. K. & Lee, Y. T. Bi-SERS sensing and enhancement by Au-Ag bimetallic non-alloyed nanoparticles on amorphous and crystalline silicon substrate. **23,** 232–240 (2015).
27. Sharma, B., Frontiera, R. R., Henry, A. I., Ringe, E. & Van Duyne, R. P. SERS: Materials, applications, and the future. *Mater. Today* **15,** 16–25 (2012).
28. Kim, W. *et al*. Low-Cost Label-Free Biosensing Bimetallic Cellulose Strip with SILAR-Synthesized Silver Core-Gold Shell Nanoparticle Structures. *Anal. Chem.* **89,** 6448–6454 (2017).
29. Oliveira, M. J. *et al*. Office paper decorated with silver nanostars-an alternative cost effective platform for trace analyte detection by SERS. *Sci. Rep.* **7,** 1–14 (2017).
30. Lee, S. Y. *et al*. Dispersion in the SERS enhancement with silver nanocube dimers. *ACS Nano* **4,** 5763–5772 (2010).
31. Cristina, A. & Araújo, J. Plasmonic Silver Nanoparticles by Dewetting process : Applications in SERS and Thin Film Solar Cells. (Faculdade de Ciências e Tecnologia e a Universidade Nova de Lisboa, 2018).
32. Alvarez-Puebla, R. A. & Liz-Marzán, L. M. Traps and cages for universal SERS detection. *Chem. Soc. Rev.* **41,** 43–51 (2012).
33. Csapó, E. *et al*. Synthesis and characterization of Ag/Au alloy and core(Ag)-shell(Au) nanoparticles. *Colloids Surfaces A Physicochem. Eng. Asp.* **415,** 281–287 (2012).
34. Hamidi-Asl, E., Dardenne, F., Pilehvar, S., Blust, R. & De Wael, K. Unique Properties of Core Shell Ag@Au Nanoparticles for the Aptasensing of Bacterial Cells. *Chemosensors* **4,** 16 (2016).
35. Khlebtsov, N. G. & Dykman, L. A. Optical properties and biomedical applications of plasmonic nanoparticles. *J. Quant. Spectrosc. Radiat. Transf.* **111,** 1–35 (2010).
36. Yang, Y., Shi, J., Kawamura, G. & Nogami, M. Preparation of Au-Ag, Ag-Au core-shell bimetallic nanoparticles for surface-enhanced Raman scattering. *Scr. Mater.* **58,** 862–865 (2008).
37. Kanniainen, T., Ihanus, J. & Leskela, M. Growth of strongly orientated lead sulfide thin films by successive ionic layer adsorption and reaction (SILAR) technique. **6,** 161–164 (1996).

38. Dietz, C. Whiteness indices and UV standards. 1–11 (2011).
39. Reed, S. Introduction to Energy Dispersive X-ray Spectrometry. *Electron probe Microanal*. 1–12 (1969). doi:S0104-66322011000100011
40. Castro, K. *et al*. Nuclear Instruments and Methods in Physics Research B Assessment of the weathering effects on cellulose based materials through a multianalytical approach. *Nucl. Inst. Methods Phys. Res. B* **269,** 1401–1410 (2011).
41. Orue, A., Santamaria-echart, A., Eceiza, A. & Arbelaiz, A. Office waste paper as cellulose nanocrystal source. **45257,** 1–11 (2017).
42. Carolina, A. & Marques, C. Desenvolvimento de um sensor colorimétrico em papel para a deteção de bactérias eletroquimicamente ativas. (A Faculdade de Ciências e Tecnologia e a Universidade Nova de Lisboa, 2014).
43. Materials, L. *Characterization of Lignocellulosic Materials 1405158808.pdf*. (2008).
44. Korotcenkov, G., Tolstoy, V. & Schwank, J. Successive ionic layer deposition (SILD) as a new sensor technology : synthesis and modification of metal oxides *. **17,** 1861–1869 (2006).
45. Lobinsky, A. A. & Tolstoy, V. P. Synthesis of γ-MnOOH nanorods by successive ionic layer deposition method and their capacitive performance. *J. Energy Chem.* **26,** 336–339 (2017).
46. González, A. L., Noguez, C., Beránek, J. & Barnard, A. S. Size, shape, stability, and color of plasmonic silver nanoparticles. *J. Phys. Chem. C* **118,** 9128–9136 (2014).
47. Han, S. W., Kim, Y. & Kim, K. Dodecanethiol-Derivatized Au / Ag Bimetallic Nanoparticles : TEM, UV/VIS, and FTIR analysis. *J. Colloid Interface Sci.* **278,** 272 (1998).
48. Sobol, P. E. & Chastain, J. *Handbook of X-ray Photoelectron Spectroscopy*. (Perkin-Elmer Corporation, 1992).
49. Smart, R., Mcintyre, S. & Bello, I. X - ray Photoelectron Spectroscopy. *Surf. Sci.* **6,** 86 (2011).
50. Thirugnanasambandan, T. & Alagar, M. Electrolytic Synthesis and Characterization of Silver Nanopowder. *Nano Biomed Eng* 1–8 (2012). doi:10.5101/nbe.v4i2.p58-65
51. Qian, Z. *et al*. Raspberry-like metamolecules exhibiting strong magnetic resonances. *ACS Nano* **9,** 1263–1270 (2015).
52. Nahar, L., Farghaly, A. A., Esteves, R. J. A. & Arachchige, I. U. Shape Controlled Synthesis of Au/Ag/Pd Nanoalloys and Their Oxidation-Induced Self-Assembly into Electrocatalytically Active Aerogel Monoliths. *Chem. Mater.* **29,** 7704–7715 (2017).
53. Giordano, L. *et al*. Observable consequences of formation of Au anions from deposition of Au atoms on ultrathin oxide films Observable consequences of formation of Au anions from deposition of Au atoms on ultrathin oxide films. **144713,** (2013).

Appendix A

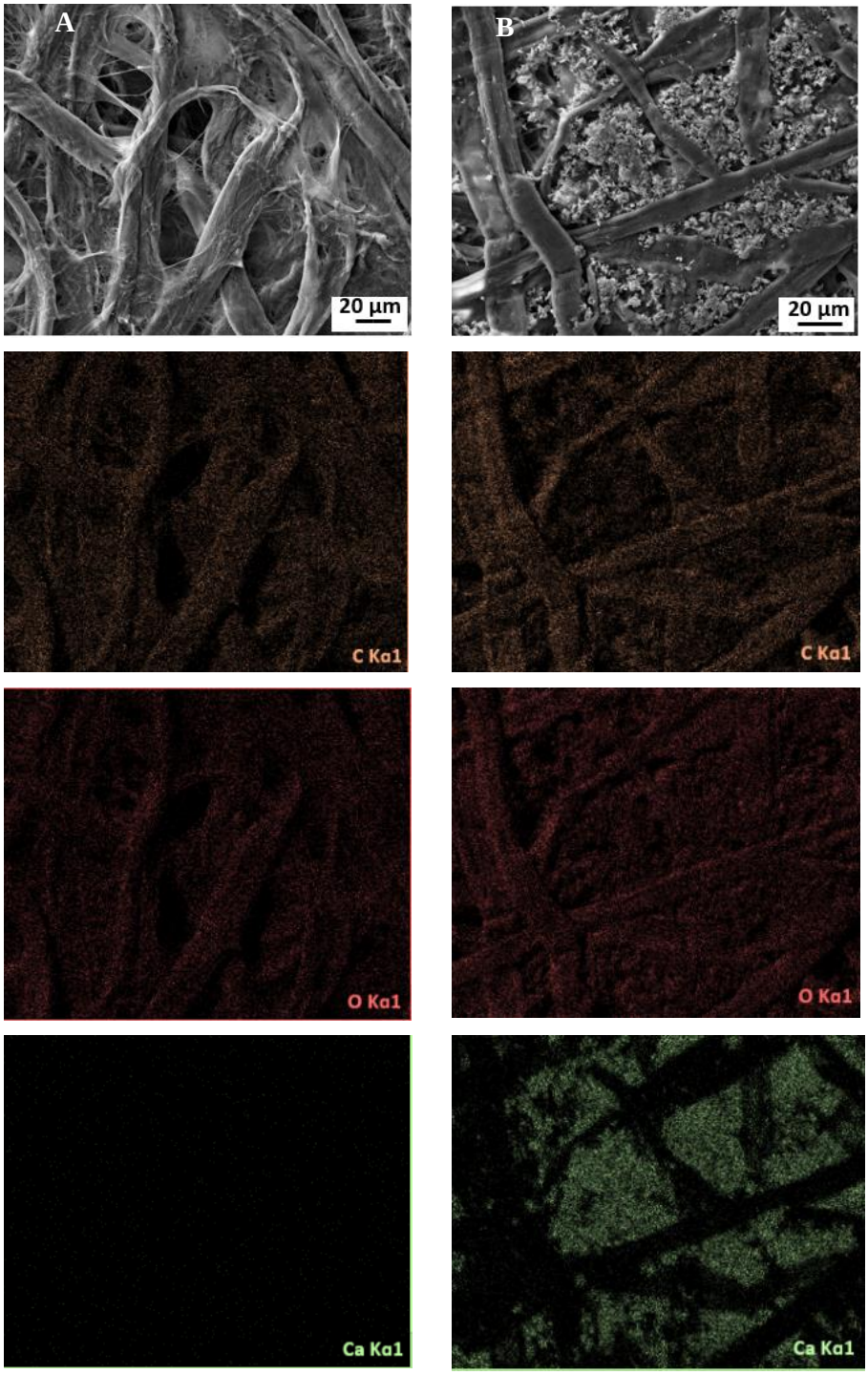

Figure A1 - EDS distribution map of A. Whatman and B. Office paper. The images were coloured artificially for easy reading

Appendix B

B1. Sucrose solution preparation:

The preparation of sucrose was made mixing 30 g of protease-free sucrose, 2.4 g of Tris-base, 50 ml of heavy water (D_2O, which must be opened in the flux. The pH value was adjusted to 7.4 with a few drops of HCl and the volume was adjusted to 100 ml with D_2O. Then it was filtered with a 0.22 µm filter vacuum inside of the flux.

B2. Measurement results by NanoSight

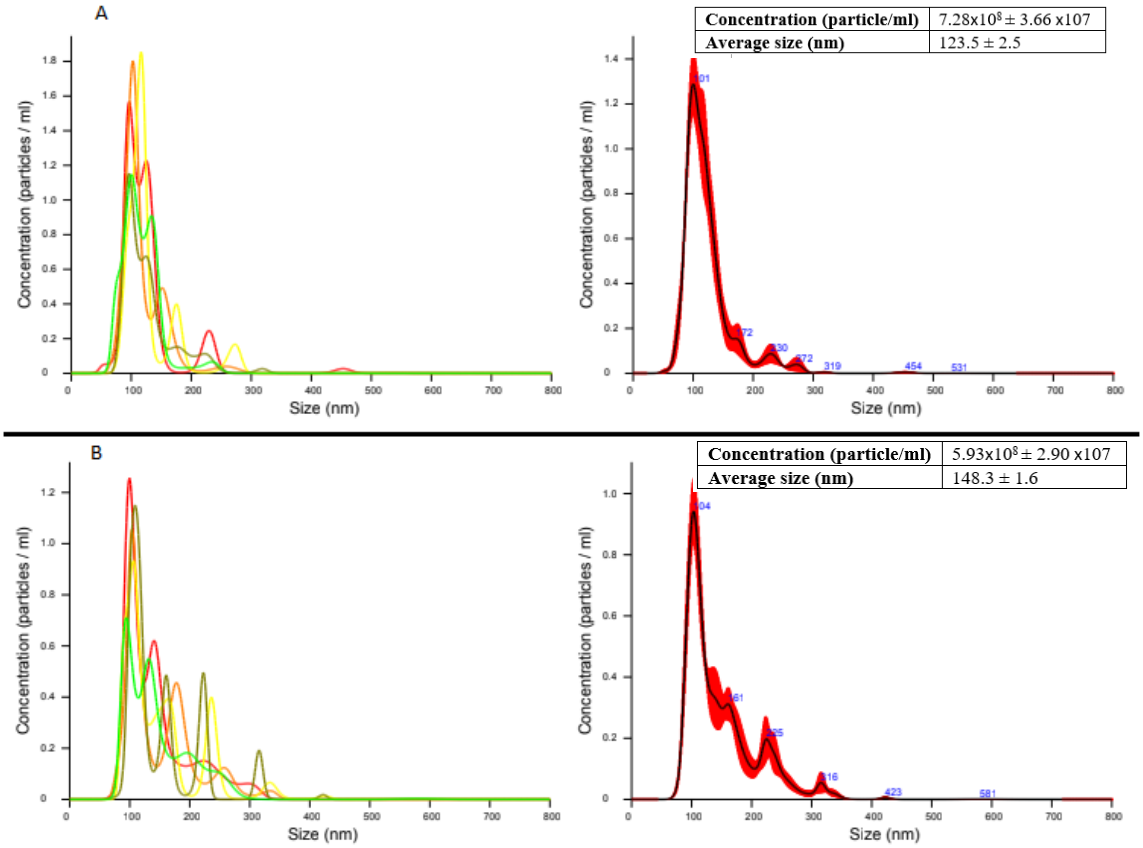

Figure B2.1 - NanoSight measurements results of exosomes from tumoral cells (A)- MDA-MB-231- and from non-tumoral cells (B)- MCF-10A. In the spectrum of the left one is represented each capture (total of 5) and in the spectrum of the right one is represented the average of the captures and the respective standard deviation. The inset represents de concentration and the average size of the exosomes.

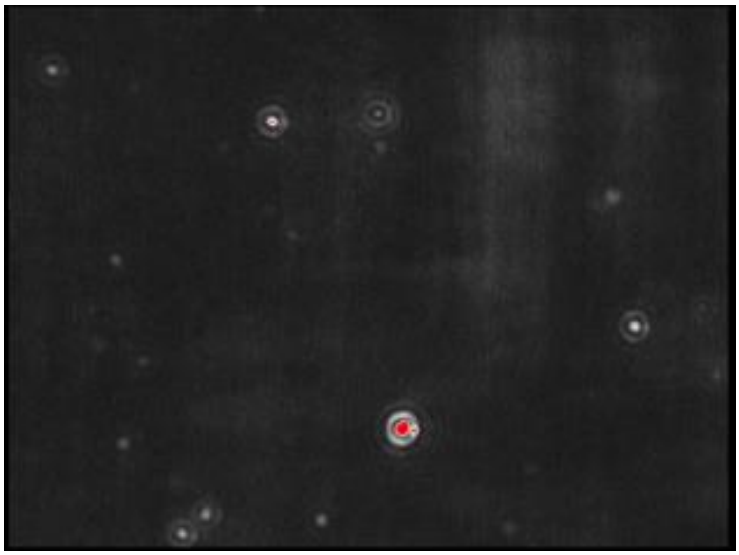

Figure B2.2 - Capture of NanoSight measurements: red points indicates particles interacting with the laser

Appendix C

C1. Different SILAR-cycles of 10/10 mM of $HAuCl_4$/$NaBH_4$

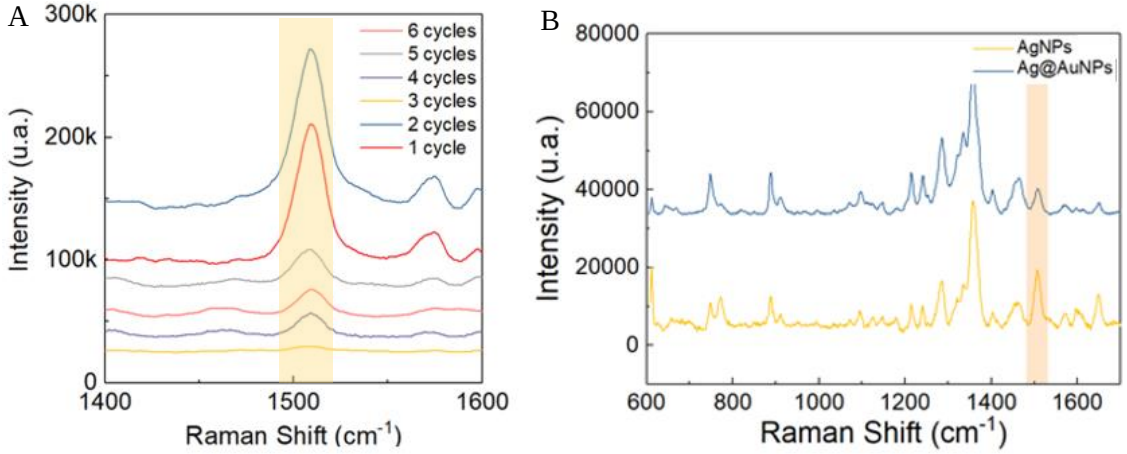

Figure C1 - (A) An increase on the SERS efficiency of bimetallic Ag@AuNPs with increasing the number of gold SILAR cycles and (B) low SERS efficiency of bimetallic Ag@AuNPs compared to monometallic AgNPs, due to the selection of improper concentrations for two SILAR reagents. A rhodamine 6G (R6G) was used as Raman probe.

By using 10 mM gold salt concentration HAuCL4 and NABH4, increasing the number of cycles of synthesis the SERS signal is also increasing (**Figure C2 (A)**). However this effect was likely to be induced by only gold nanostructure rather than bimetallic nanostructure (**Figure C2 (B)**). This finding was responsible that, although the concentration of gold ions ($HAuCl_4$) was smaller than that of silver ions ($AgNO_3$), the size of the AuNPs was greater than the AgNPs.

Therefore, the AuNPs mainly contributed the SERS effect, which they led to a low Raman intensity compared to the AgNPs. New gold salt concentrations has to be found.

C2. Raman and SERS spectra of R6G 10^{-2} and 10^{-6} M

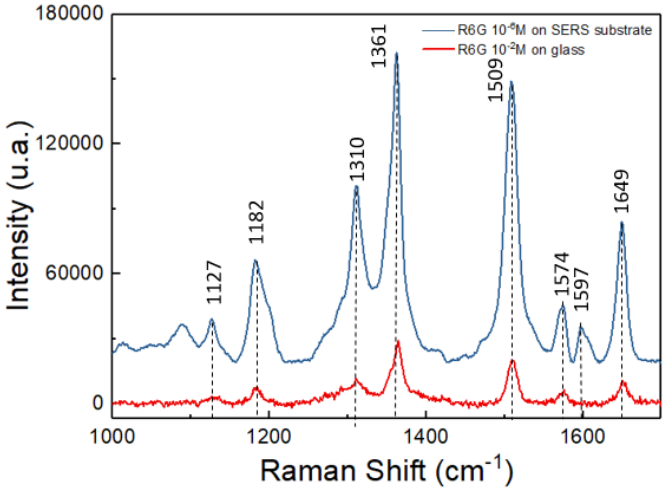

Figure C2 - Raman spectrum of R6G 10^{-6} M R6G measured on SERS substrate (blue) and 10^{-2} M measured on glass (red)

C3.Comparison of the R6G 10^{-6} M spectra of the Whatman nº1 and Office paper

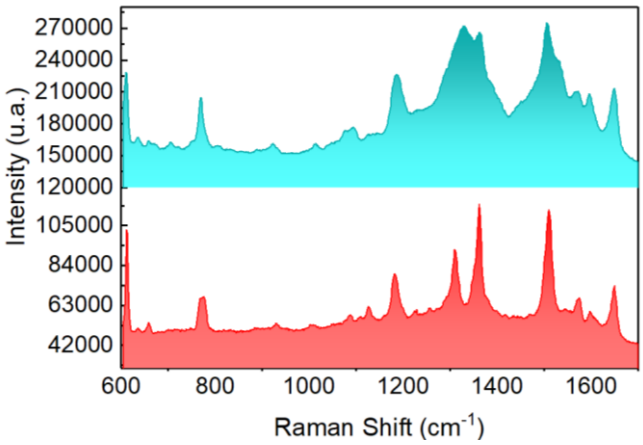

Figure C3 - Comparison of the rhodamine spectra of the Whatman nº1 and Office paper, with Ag@AuNPs SILAR-synthesized. Ag@AuNPs synthesized directly on office paper, the reducing agent of silver being the salt present in the paper and 40 secs of each cycle step (red). Ag@AuNPs synthesized directly on whatman paper, with $NaBH_4$ as AgNPs reducing agent and normal conditions (blue).

C4. Stability tests of office paper

Figure C4 represent stability tests made in Office paper with Ag@AuNPs SILAR-synthesised without $NaBH_4$ as AgNPs reducing agent, through 3 months. Measurement conditions were kept the same for direct comparation. R6G 158 cm^{-1} peak is observable until 2 months after substrate fabrication, with noticeable peak intensity changes, which is seen to be a large reduction in peak

intensity. However, for 3 months, the substrate does not show peak at 1508 cm^{-1}, which indicates substrate degradation.

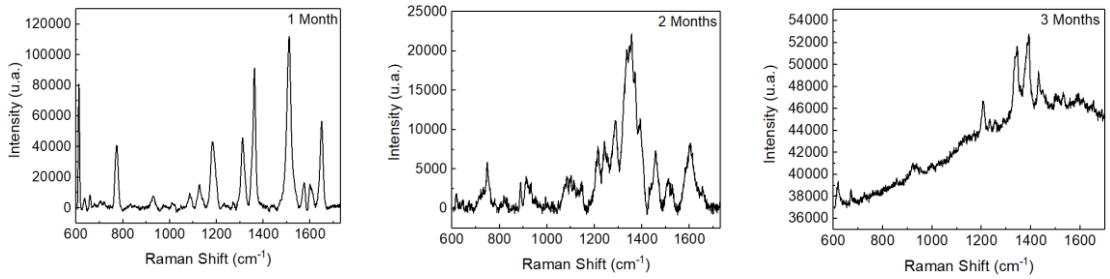

Figure C4 - Stability tests on Office paper with Ag@AuNPs SILAR-synthesised without $NaBH_4$ as AgNPs reducing agent

Appendix D

D1. Auger Parameters calculation

Auger parameters (α) were calculated from the samples in order to determine if the detected silver and gold was part of the $AgNO_3$ and $HAuCl_4$ remains or indeed Ag^0 and Au^0 nanoparticles. The obtained values (**Table D1**) were compared to literature (**Table D2**).

Table D1. Ag 3d/52 binding energies and Ag 3d5/2 – Ag M4N45N45 Auger parameters between different states of silver (adopted from *D. Wagner et. al., 2003*).

Species	3d5/2 B.E. (eV)	St. Dev.	# of Cit.	Auger Parameter	St. Dev.	# of Cit.
Ag	368.2	0.1	22	726.1	0.1	8
Ag2O	367.9	0.3	7	724.4	0.1	2
AgO	367.6	0.4	6	724.5	0.3	3
Ag2CO3	367.7	0.2	3	723.1		1
AgSO4	367.9	0.3	4	722.7	0.3	3
Ag2S	368.1	0.1	4	724.8	0.1	2
AgCl	368.1	0.0	2	723.5		1
AgF	367.8	0.1	3	722.8		1
AgF2	367.3		1			
AgI	367.9	0.2	4	724.0		1
AgNO3	368.2	0.0	2	723.8		1
AgPO3	368.3		1			

Table D1.2 - Calculated Auger parameters from different SERS substrates: Whatman and Office paper with Ag@Au bimetallic nanoparticles.

Auger Parameters			
Whatman paper		**Office paper**	
Silver	**Gold**	**Silver**	**Gold**
725.64	2099.08	725.10	2099.23

Auger parameter from the analysed samples was calculated using the kinetic energy of the smaller Au and Ag MNNa peak (due to being more well-defined) and the binding energy of the most intense Ag 3d and Au 4f peaks. By analysing the two tables it's possible to conclude that Ag or Ag2O could be present due to the proximity of Auger parameters. Also, we can eliminate the suspicion that there is no silver salt remains.

By measuring the difference between the binding energy of the Au 4f photoelectron species (83.9 eV and 83.8 eV related to Whatman and Office paper, respectively) and the kinetic energy of the M5N67N67 transition (2015.61 eV) the experimental a was 2099.08 eV for Whatman paper and 2099.23 eV for Office paper, which is in agreement with Au foil (2099.15 eV) indicating that the structures were predominantly metallic[53].

D2. 2θ of the diffractions of silver and gold structures

Table D2 - The 2θ values and corresponding diffractions of silver and gold crystals in XRD analysis

Type of paper	Ag (2θ)	XRD analysis	Au (2θ)	XRD analysis
Whatman nº1	38.1 º	(111)	-	-
Office paper	38.1 º	(111)	44.3 º	(200)
	64.5 º	(220)	64.7 º	(220)
	77.5 º	(311)		

D3. SEM-EDS results of the bimetallic nanoparticles synthesized on different papers

Table D3 - SEM-EDS results of Ag@AuNPs synthesised on Whatman paper with the previously optimized SILAR-synthesis.

Element	Line type	Apparent Concentration	Atomic %
C	K series	3.62	66.75
O	K series	2.64	32.86
Ag	L series	0.11	0.20
Au	M series	0.18	0.18
			100

Table D3.1 - SEM-EDS results of Ag@AuNPs SILAR-synthesised on Office paper with 40 secs each cycle step.

Element	Line type	Apparent Concentration	Atomic %
C	K series	3.66	60.22
O	K series	2.50	31.59
Ag	L series	4.91	7.14
Au	M series	1.27	1.05
			100

Appendix E

In this appendix are presented figures related to PCA measurements and analysis of the raman spectra corresponding to the analysed samples

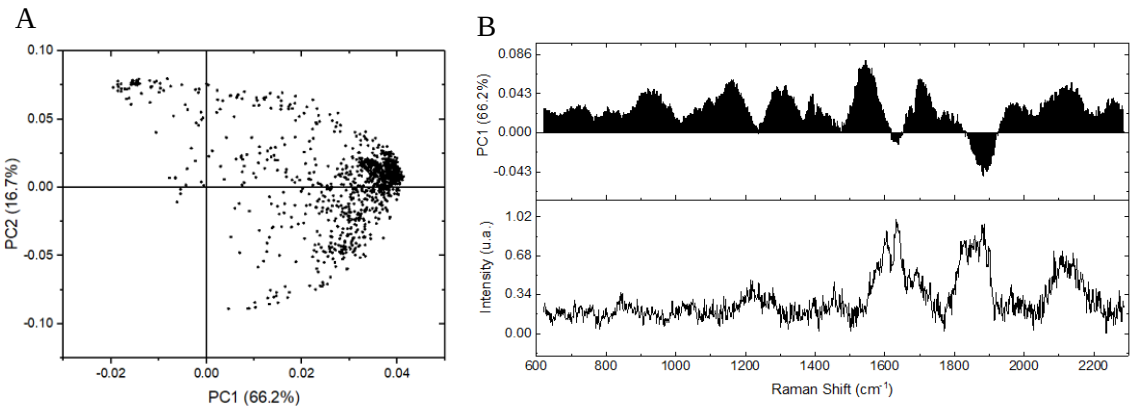

Figure E1 - A- Loading plot obtained from PCA analysis of tumoral and non-tumoral exosomes on Office paper with Ag@AuNPs SILAR-synthesized without $NaBH_4$ as AgNPs reducing agent and 40 secs each Ag cycle stpe; B- Average tumoral exosome spectra and each peak variance contribution to the PC1.

The loading plots helps to understand the wavenumbers that most contribute to the variance. Observing the two plots it's possible to observe that practically the whole equally contributes spectrum for PC1 (**Figure E1**).

E2. Proof of concept analysis

As proof of concept, a sample was introduced, whose origin is known, in the obtained score plot and the results are represented in the **Figure E2** and **E3**.

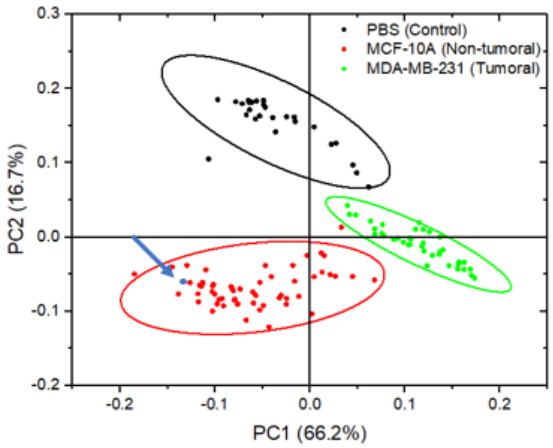

Figure E2 - PCA calibrated score plot with a non-tumoral sample serving as proof of concept. Control (black), tumoral (green), non-tumoral (red) and sample (blue).

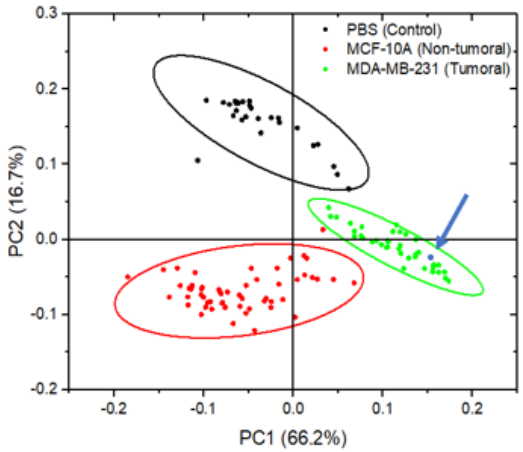

Figure E3 - PCA calibrated score plot with a tumoral sample serving as proof of concept. Control (black), tumoral (green), healthy (red) and sample (purple).

In this case we can affirm with 95% certainty that the samples analyzed non-tumoral (E2) and tumoral (E3) belong to the groups surrounded by the ellipses, demonstrating that this is a viable point of care diagnosis.